Fatigue Crack Growth in 7475-T651 Aluminum Alloy Plate in Hard Vacuum and Water Vapor

By

Dennis L. Dicus

B.S. June 1966, Tennessee Technological University

A Thesis submitted to

The Faculty of

The Graduate School of Engineering and Applied Science

of The George Washington University in partial satisfaction

of the requirements for the degree of Master of Science

November 1981

ABSTRACT

An investigation has been performed to assess the effects of water vapor on fatigue crack growth in 7475-T651 aluminum alloy plate and to determine whether these effects are frequency dependent. Twenty-five mm thick compact specimens were subjected to constant amplitude fatigue testing at a load ratio of 0.2. Fatigue crack growth rates were determined at frequencies of 1 Hz and 10 Hz in hard vacuum and laboratory air and in mixtures of water vapor and nitrogen at water vapor partial pressures ranging from 94 Pa to 3.8 kPa.

A significant effect of water vapor on fatigue crack growth rates was observed at the lowest water vapor pressure tested, but little change in cracking rates occurred for water vapor pressures up to 1.03 kPa. However, an abrupt acceleration of cracking rates was observed at higher water vapor pressures. At low stress intensity factor ranges cracking rates at the lowest and highest water vapor pressure tested were, respectively, two times higher and five times higher than rates in vacuum. Although a frequency effect was observed in laboratory air, cracking rates in water vapor and vacuum were insensitive to a ten fold change in frequency.

Fracture surfaces of specimens tested in water vapor and vacuum exhibited different amounts of residual deformation. Reduced deformation on the fracture surfaces of specimens tested in water vapor suggests embrittlement of the plastic zone ahead of the crack tip as a result of environmental interaction.

ACKNOWLEDGEMENTS

The author acknowledges the guidance of his advisor, Mr. W. Barry Lisagor, and thanks him for his support, helpful criticisms, and suggestions. The author also thanks Mrs. Elsie Illg for her assistance with scanning electron microscopy and metallography. Appreciation is expressed to the National Aeronautics and Space Administration, Langley Research Center for permitting this research to be conducted as a part of the author's work assignment. Finally, the author thanks his wife, Kathryn, and children, Mark and Susan, for their patient understanding and constant support.

TABLE OF CONTENTS

SYMBOLS

a	crack length, m
b_j	coefficients in compliance calibration equation
B	thickness of compact specimen, m (See fig. 5.)
C	constant in fatigue crack propagation equations
da/dn	fatigue crack growth rate, m/cycle
$(da/dN)_e$	fatigue crack growth rate in an agressive environment, m/cycle
$(da/dN)_r$	fatigue crack growth rate in an inert environment, m/cycle
$(da/dN)_{SCC}$	portion of fatigue crack growth rate in an agressive environment due to stress corrosion cracking, m/cycle
da/dt	crack velocity under constant load in an agressive environment, m/s
E	modulus of elasticity, Pa
f	frequency, Hz
H	half height of compact specimen, m (See fig. 5.)
i,j	indices
K	stress intensity factor, $N/m^{3/2}$
K_c	plane stress fracture toughness, $N/m^{3/2}$
K_{Ic}	plane strain fracture toughness, $N/m^{3/2}$
K_{ISCC}	threshold stress intensity factor for stress corrosion cracking, $N/m^{3/2}$
K_{max}	maximum stress intensity factor in fatigue cycle, $N/m^{3/2}$

K_{th}	threshold stress intensity factor for fatigue crack growth, $N/m^{3/2}$
ΔK	stress intensity factor range in fatigue cycle, $N/m^{3/2}$
ΔK_o	initial stress intensity factor range, $N/m^{3/2}$
m,n	constants in fatigue crack propagation equations
N	number of load cycles
P	applied load, N
ΔP	load range in fatigue cycle, N
r	distance from the crack tip to the location where σ_y is calculated, m
R	ratio of minimum stress to maximum stress or minimum load to maximum load
S	remote stress, Pa
V	crack-opening displacement at the crack mouth of compact specimen, m
ΔV	crack-opening displacement range in fatigue cycle, m
W	width of compact specimen, m (See fig. 5.)
ν	Poisson's ratio
σ_y	principal stress normal to the crack plane, Pa

INTRODUCTION

Corrosion fatigue, the response of a material to the combined actions of cyclic stress and a corrosive environment, is recognized as a principal factor in accelerating structural degradation of aerospace vehicles in service. A lack of understanding of the fundamental mechanisms involved in chemical/mechanical environment interactions has seriously limited consideration of corrosion fatigue in the structural design process and in alloy development. Whereas test techniques to characterize strength, fracture toughness, and fatigue resistance are well understood and the data are useable by the designer, the effects of corrosion receive scant attention in the design process. Although test techniques are available to characterize the susceptability of a material to stress corrosion cracking (SCC), these data are often not relatable to design for real service environments. As a result alloy selection and structural design are based upon a qualitative judgment of immunity to SCC. In the case of corrosion-fatigue, materials are not systematically characterized with respect to this phenomenon; therefore, corrosion fatigue is only addressed on an after-the-fact basis.

Even though fatigue is treated as a purely mechanical phenomenon, it has received primary attention in the structural design of aerospace vehicles. Concern with fatigue has resulted in the development of two structural design philosophies: (1) safe-life design and (2) fail-safe design. Safe-life design, which is the older design philosophy, is mostly concerned with the crack initiation phase of the fatigue process and is based on precluding the development of a crack of significant size

and thus preventing fracture during the operational lifetime of a component (ref. 1). With the knowledge that structures are never truly flaw free and that fatigue cracks tend to initiate very early in the life of complex structures at discontinuities such as holes, fillets and other abrupt changes in configuration, the fail-safe design philosophy emerged. Predominantly concerned with the crack propagation stage of the fatigue process, fail-safe design emphasizes redundant load paths and utilizes periodic inspections to detect the existence of cracks. Crack growth predictions are employed to determine the safe inspection interval and to insure that fracture will not occur between inspections (ref. 2). Modern aerospace structural design, generally known as damage-tolerant design, tends to combine aspects of both the safe-life and the fail-safe philosophies (refs. 1-3). In choosing a material the designer is concerned with the ability of the material to resist both crack initiation and crack propagation.

Aluminum alloys have been the most widely used materials of aircraft construction for more than 40 years. The most commonly used alloys have been 2024 and 7075 in a variety of heat treatments. In the T6 condition 7075 possesses superior ambient temperature tensile properties, but its fracture toughness and fatigue resistance are inferior to lower tensile strength 2024-T3. The development of improved alloys for aerospace application has tended to emphasize modifications of these two workhorse alloys in an attempt to produce a better balance of properties through more tightly controlled chemistry. Containing substantially lower amounts of the impurity elements Si, Ti, Fe, and Mn, one of these new

alloys, 7475, is an improved chemistry modification of 7075. In the T6 condition 7475 combines tensile properties comparable with those of 7075-T6 with fracture toughness and fatigue resistance comparable to 2024-T3. Because of its excellent balance of properties, 7475 is expected to be widely used in future aerospace vehicles.

The fact that air accelerated the fatigue-failure of aluminum alloys was first reported in the literature almost 50 years ago (ref. 4). Early research was largely limited to the effects of air and its constituents on total fatigue life (refs. 4-7). With the development of linear elastic fracture mechanics and fail-safe design philosophy, research emphasis shifted to studies of the crack propagation phase (refs. 8-12). Although the effects on crack initiation are disputed, there is general agreement in the literature that water vapor has a greater effect on fatigue crack growth rates in aluminum alloys than the other constituents of pure air. The present study was undertaken to assess the effects of water vapor on fatigue crack growth in 7475-T651 aluminum alloy plate and to determine whether these effects are frequency dependent. Fatigue crack growth rates were determined at frequencies of 1 and 10 Hz in hard vacuum and laboratory air and in mixtures of water vapor and nitrogen at various partial pressures of water vapor. Fracture surfaces were characterized in an attempt to correlate fracture morphology with environmental interaction.

REVIEW OF LITERATURE AND THEORY

The phenomenon of fatigue in metals is generally divided into three sequential phases: crack initiation, crack propagation, and final fracture. The crack initiation phase begins with the first load cycle and includes limited microcracking along slip bands or grain boundaries (refs. 13-15). Although the dividing line between the initiation and propagation phases is not well defined, the crack propagation phase is generally thought to have begun once a macroscopic crack has developed and involves all the remaining life except for the last few loading cycles. The final fracture phase involves only the last few loading cycles during which final failure of the material occurs when a combination of crack size and load reaches a critical value producing gross mechanical instability.

Historically, research on corrosion fatigue has paralleled research on fatigue per se. Early research on corrosion fatigue was largely limited to effects on total fatigue life. With the advent of linear elastic fracture mechanics, research emphasis shifted primarily to studies of the crack propagation phase. Less research has been carried out on the crack initiation phase primarily because of the experimental difficulties involved and the lack of an adequate definition of the boundary between the crack initiation and propagation phases. Research on the crack propagation phase has received added impetus from the fact that engineering structures are never truly flaw free and that cracks tend to initiate very early in the life of complex structures. This

literature review will be largely limited to the crack propagation phase of corrosion fatigue when a macroscopic crack is growing.

Fracture Mechanics

Based on the pioneering work of Griffith (ref. 16), Irwin (ref. 17) and Williams (ref. 18) independently discovered the fundamental concept of fracture mechanics: the stress near the tip of a crack in an elastic body of arbitrary shape and loading varies in a simple way with position relative to the crack tip. Complete specification of the stress, strain and displacement requires three scaling factors which are determined by the geometry and load. These three scaling factors are related to the three possible modes of motion between the faces of the crack. The numerical coefficients giving the magnitude of each of these three modes of motion are called stress intensity factors. Direct separation of the crack faces symmetrically with respect to the plane of the crack is known as the opening mode or mode 1. For a crack of length, 2a, in an infinitely wide elastic plate subjected to a uniform remote stress, S, the mode 1 stress intensity factor is given by

$$K = \lim_{r \to 0} [\sigma_y \sqrt{2\pi r}] = S\sqrt{\pi a} \qquad (1)$$

where r is the distance from the crack tip to the location where the principal stress normal to the crack plane σ_y, is calculated.

Equation (1) indicates that for a sharp crack as the radius approaches zero, the stress would be infinite at the crack tip. In reality the crack will always have a finite radius of curvature, and the

stress, although very large, will remain finite. Unless the material is completely brittle, yielding will occur, and this local plastic deformation will tend to reduce the stress concentration effects of the crack. As long as the plastic zone is small in comparison with the crack length and other dimensions of the body, the elastic solution represents a reasonably accurate approximation of the stress and displacement near the crack tip. Since the small plastic zone at the crack tip is contained within the surrounding elastic material, it is reasonable to expect that the behavior of the plastic zone can be characterized by the stress intensity factor.

When the combination of crack length and shape and applied load produce a critical value of the stress intensity factor, a material will undergo crack extension. The critical stress intensity factor is a measure of the fracture toughness of a material and is a function of the degree of constraint at the crack tip. Under plane strain conditions which generally occur in thick sections, the critical stress intensity factor is a material property, K_{Ic}, the plane strain fracture toughness. Valid determinations of K_{Ic} require that the plastic zone be very small in relation to crack length and specimen dimensions so that plane strain conditions are closely approximated. Although pure plane stress conditions only occur in very thin sections, K_c, the plane stress fracture toughness, is often determined under crack tip constraint conditions which are intermediate between plane stress and plain strain. As a result, values of K_c are dependent on specimen geometry.

Fatigue Crack Propagation Models

Many crack propagation models have been proposed which utilize the stress intensity factor to characterize the crack driving force under a variety of loading conditions and geometrical configurations. In all of these models, crack propagation rate was assumed to be a continuous function of loading, geometrical configuration, and material properties. The ensuing discussion of some of the commonly used models is based on the presentation by Newman in reference 19 and will be limited to constant-amplitude loading where the effects of prior load history need not be considered. In this paper the terms fatigue crack propagation rate, fatigue crack growth rate, and cracking rate are used synonymously.

Paris, Gomez, and Anderson (ref. 20) suggested that the stress intensity factor, K, not only characterized the stress state in the vicinity of the crack tip but would also account for the effects of specimen loading on fatigue crack propagation rates. Paris and Erdogan (ref. 21) analyzed various crack propagation models and determined that fatigue crack propagation rate was best represented by the equation

$$da/dN = CK^n \tag{2}$$

where C and n are empirical constants. Subsequently, Paris (ref. 22) proposed that fatigue crack propagation rate was a function of ΔK, the stress intensity factor range. Thus,

$$da/dN = C\,\Delta K^n \tag{3}$$

where C and n are again empirical constants. Using the equation to

analyze data on steel, titanium, and aluminum, he suggested that the value of the exponent n was approximately four. Hudson and Scardina (ref. 23) determined that the constant C varied with R, the ratio of minimum stress to maximum stress.

Forman, Kearney, and Engle (ref. 24) proposed that fatigue crack propagation rate was a function of K_c, the plane-stress fracture toughness of the material, as well as the stress intensity factor range and the stress ratio. Their empirical equation has the form

$$da/dN = \frac{C\,\Delta K^n}{(1-R)K_c - \Delta K} \tag{4}$$

where C and n are empirical constants.

Erdogan (ref. 25) developed a model assuming small scale yielding. He proposed that fatigue crack propagation rate was a function of both the maximum stress intensity factor, K_{max}, and the stress intensity factor range such that

$$da/dN = C\,\Delta K^m K_{max}^n \tag{5}$$

where c, m, and n are all empirical constants.

Hudson (ref. 26) studied the effect of stress ratio on fatigue crack propagation in two aluminum alloys and correlated the data using equations (3), (4), and (5). His data covered a wide range of stress ratios and maximum stress levels in 7075-T6 and 2024-T3. Forman's equation produced an excellent fit to all the data. Erdogan s and Paris'

equations showed good correlation with the data except at the higher growth rates in 7075-T6.

The foregoing crack propagation models primarily incorporate the effects of various loading variables on fatigue crack growth. They were developed without regard to environmental influences on crack growth, and, by and large, the experiments on which they were based were performed with no environmental control. However, for a single material and environment combination, fatigue crack growth rates can generally be plotted with equal success against either ΔK or K_{max}, with all data generated at a single stress ratio falling within a narrow scatter band. When more than one stress ratio is included, a systematic ordering of the data with stress ratio usually occurs (refs. 24, 26).

Relationships Between Corrosion Fatigue, Fatigue and Stress Corrosion Cracking

Corrosion fatigue, the response of a material to the combined actions of cyclic stress and a corrosive environment, can be put in perspective by examining its relationships with purely mechanical fatigue and SCC. Figure 1, which is patterned after an illustration in reference 27, shows the crack growth response resulting from these related phenomena as a function of stress intensity. The relationship between corrosion fatigue and purely mechanical fatigue is schematically illustrated in figure 1a which compares the fatigue crack growth response of a material in inert and aggressive environments. Fatigue crack growth rate, da/dN, is plotted as a function of K_{max} at $R = 0$. (Note that for $R = 0$, $K_{max} = \Delta K$.) On such a plot the fatigue crack growth

response can generally be divided into three regions. The response in region I is associated with K_{th}, an apparent threshold value of K below which no fatigue cracking can occur. In region II the cracking rate is dependent on some power of K; that is, cracking rate appears to follow the Paris model, equation (3). The response in region III is dominated by the rapid approach of K_c where unstable cracking occurs leading to fracture. The effects of an aggressive environment on fatigue crack growth include a possible reduction of K_{th} but are primarily evidenced by an acceleration of da/dN in regions I and II. In region III environmental effects on da/dN are diminished as K_{max} approaches K_c. Environmental effects on da/dN are also a function of loading frequency. As indicated in figure 1a, a lower frequency, f, generally results in a greater acceleration of da/dN. Conversely, as frequency is increased, environmental effects on da/dN are diminished and may be completely eliminated at high frequency (ref. 28).

The SCC behavior of the same material in the same aggressive environment is schematically depicted in figure 1b. Crack velocity, da/dt, is plotted as a function of K for a precracked specimen held at constant load in the aggressive environment. Like fatigue crack growth, SCC response can be divided into three regions. In region I the response is strongly dependent on K and exhibits an apparent threshold K value, K_{ISCC}, below which no SCC takes place. Region II is known as the K insensitive region where da/dt is largely independent of K level and may be limited by the corrodent transport process. In region III da/dt is again strongly dependent on K and increases rapidly as K

approaches K_c. A comparison of figures 1a and 1b indicates that both purely mechanical fatigue and corrosion fatigue occur at K_{max} values less than K_{ISCC}. Environmental acceleration of fatigue crack growth at K levels less than K_{ISCC} has been reported for aluminum, magnesium, and titanium alloys and steels exposed to a variety of environments (refs. 29-31). In fact, corrosion fatigue of a material can occur in an environment in which the material is essentially immune to SCC (ref. 29).

Corrosion fatigue has been modeled by superposition of SCC and purely mechanical fatigue crack growth (refs. 32-33). Wei and Landes (ref. 32) proposed that the fatigue cracking rate for a material in an aggressive environment, $(da/dN)_e$, was the sum of the fatigue cracking rate in an inert environment, $(da/dN)_r$, and the contribution of SCC in the same aggressive environment, $(da/dN)_{scc}$. That is

$$(da/dN)_e = (da/dN)_r + (da/dN)_{scc} \tag{6}$$

where

$$(da/dN)_{scc} = \int_0^{1/f} \left[\frac{da}{dt} (K) \right] dt$$

Such linear superposition models were not proposed to account for all observed corrosion fatigue behavior, but equation (6) does approximate observed trends in a few material environment combinations at K-levels in excess of K_{ISCC} (refs. 32-34). However, as indicated in figure 1 environmental effects on fatigue crack growth rates exist at K-levels less than K_{ISCC}. In this regime linear superposition does

not apply because corrosion and mechanical fatigue are interacting. An abrupt cessation of these interactions at or near K_{ISCC} seems unlikely since region II corrosion fatigue spans a range of K above and below K_{ISCC} with no apparent discontinuity in crack growth rates (ref. 29). The superposition concept may also be unsatisfactory for materials which exhibit different fracture modes under different loading conditions. For example, aluminum alloys usually fracture intergranularly under stress-corrosion conditions, but they often fracture transgranularly under corrosion fatigue conditions (refs. 27, 29).

McEvily and Wei (ref. 35) suggested that environmental effects on fatigue crack growth could be grouped into three basic types of response displayed by different material-environment combinations. These three types of behavior are illustrated in figure 2 which is redrawn from reference 35. Type A behavior which is typified by the aluminum-water system shows an apparent reduction in K_{th} and continuously higher growth rates until K approaches K_c. This type of environmental effect results from the synergistic action of corrosion and fatigue. Type B behavior, typified by the hydrogen-steel system, shows an environmental effect with a substantial SCC component and no interaction between corrosion and fatigue. The environmental effect is confined to the region where K exceeds K_{ISCC}. Type C represents the behavior of many material-environment systems which display type A behavior below K_{ISCC} and type B behavior above.

Influence of Water Vapor on Fatigue Crack Propagation in Aluminum Alloys

Many variables affect the influence of water vapor on fatigue crack propagation in aluminum alloys. These variables generally are of three types: mechanical, environmental, and metallurgical. The mechanical variables are related to loading conditions and specimen or component geometry. The general effects of some of the more important mechanical variables including ΔK and R have been discussed in a preceeding section. For corrosion fatigue experiments low values of R are generally used. Environmental variables include composition, temperature, pressure, and whether the environment is static or circulating. Metallurgical variables include alloy composition, heat treatment, microstructure, and mechanical properties. This listing is by no means all encompassing but is provided to demonstrate the broad range of factors and their interaction in the corrosion fatigue process. To better define the influence of water vapor, the review which follows will include the influence of other environments such as air and vacuum on the fatigue of aluminum alloys. The review will focus on the effects of selected variables and conclude with a discussion of mechanisms.

Effects of vacuum, air and its constituents.- The effects of vacuum and air and its principal constituents on the fatigue of aluminum alloys have been studied extensively. Wadsworth and Hutchings (ref. 5) showed that for pure aluminum total fatigue life in a vacuum of 1.3 mPa was five times greater than life in air at normal atmospheric pressure. They reported that crack propagation occupied about 90% of total fatigue

life in both environments and concluded that the environmental effect was restricted to the rate of crack propagation. Although their conclusion that crack initiation is unaffected in air versus vacuum has not been generally accepted (ref. 36), their findings that the presence of air reduces total fatigue life and increases the rate of crack propagation in aluminum and its alloys have been confirmed by many researchers (refs. 4, 6-8, 10, 37).

Several investigations have been performed to determine the effect of decreasing pressure on total fatigue life and fatigue crack propagation rate. Wadsworth and Hutchings (ref. 5), Hudson (ref. 37), Snowden (ref. 38), and Christensen (ref. 39) reported a continuous increase in the fatigue life of pure aluminum and 2014-T6 and 7075-T6 aluminum alloys as gas pressure was reduced from normal atmospheric levels to hard vacuum. Other investigators, including Ham and Reichenbach (ref. 40), Hordon (ref. 41), Shen, Podlaseck, and Kramer (ref. 42), and Shen (ref. 43), have reported a discontinuous or stepped variation in the fatigue life of pure aluminum and aluminum alloy 1100-H14 with decreasing gas pressure. All of these latter investigators found fatigue life to be nearly independent of pressure over the range from atmospheric levels to approximately 13 Pa, to increase steadily over the approximate range from 13 Pa to 13 mPa, and to be again nearly independent of pressure from 13 mPa down to 1.3 μPa. Commensurate with these fatigue life results, fatigue crack propagation rates are decreased at reduced pressure, particularly at low values of ΔK. Hordon (ref. 41) found that in aluminum alloy 1100-H14 the ratio of the

fatigue crack propagation rates at low ΔK in a vacuum of 26 μPa versus air at atmospheric pressure was about 1/10. Hudson (ref. 37) reported that for 7075-T6 the fatigue crack propagation rate in a vacuum of 7 μPa was about one-half of the rate measured at atmospheric pressure. Bradshaw and Wheeler (ref. 10) found that in a vacuum of 4 μPa fatigue crack propagation rates at low ΔK in DTD 5070A (clad Al-Cu-Mg alloy) and DTD 683 (Al-Zn-Mg-Cu alloy) were, respectively, 1/7 and 1/60 of the rates in air at atmospheric pressure.

Dry noble gases such as nitrogen and argon are generally considered to have no detrimental effects on fatigue in aluminum alloys. Broom and Nicholson (ref. 7) reported that fatigue lives of thre aluminum alloys were from 6 to 10 times greater in dry nitrogen than in air at atmospheric pressure. They found that the fatigue life of an Al-4% Cu alloy was roughly the same in dry nitrogen as in a vacuum of 260 μPa. Bradshaw and Wheeler (ref. 12) found only minor differences between fatigue crack propagation rates in dry nitrogen and in a vacuum of 4 μPa in aluminum alloys DTD 5070A and DTD 683. While specific investigations of the effects of dry argon versus hard vacuum on aluminum alloys cannot be cited from the literature, fatigue crack propagation rates in these two environments are roughly equivalent. In practice both dry argon and hard vacuum are employed as inert reference environments.

The effect of oxygen on the fatigue of aluminum alloys has received considerable attention. Broom and Nicholson (ref. 7) found that the fatigue lives of 4% Cu, B.S. L65, and DTD 683 aluminum alloys were eight, five, and two times longer, respectively, in dry oxygen than in air at

atmospheric pressure. They also found that the fatigue life of the Al-4% Cu alloy was four times longer in dry oxygen than in oxygen with some moisture present. Wright and Hordon (ref. 44) reported that in the pressure range from 1.3 to 13 Pa oxygen and water vapor produced equally detrimental effects on the fatigue life of 1100-H14 aluminum alloy. Bradshaw and Wheeler (refs. 10, 12) found that dry oxygen had only a minor effect on fatigue crack propagation rates in aluminum alloys DTD 5070A and DTD 683 as compared to rates in hard vacuum and that this effect was limited to very low ΔK levels. However, they found that dry oxygen had a more substantial detrimental effect on cracking rates in 99.99% pure aluminum. In Alclad 2024-T3 Hartman (ref. 45) found that fatigue crack propagation rates were similar in dry oxygen and dry argon and that the rates in these dry gases were much lower than the rates in wet oxygen, wet argon, or air at 60% relative humidity. Wei (ref. 46) reported that over the temperature range from 295 to 380 K dry oxygen had little, if any, effect on fatigue crack propagation rates in 7075-T651 as compared to rates in dehumidified argon.

Summarizing the effects of vacuum and air and its constituents, air and nitrogen have no effect on fatigue crack propagation in aluminum alloys unless water vapor is also present. Fatigue crack propagation rates in dry air, dry nitrogen, and dry argon are similar to the rates observed under hard vacuum. Except in pure aluminum and the commercially pure 1100 alloy, dry oxygen also appears to have little effect. Acceleration of aluminum alloy fatigue crack propagation in wet air, wet nitrogen, and wet oxygen appears to be caused solely by the presence of

water vapor; none of the evidence suggests that mixtures of water vapor and the other gases produce strong synergistic effects.

Effect of concentration or pressure of water vapor.- Several investigations have been performed on the effects of the concentration or partial pressure of water vapor in various gaseous environments and the pressure in a pure water vapor environment. Hartman, et al. (ref. 8) and Hartman (ref. 45) studied the effects of relative humidity in air at normal atmospheric pressure on fatigue crack propagation rates in 7075-T6 and 2024-T3. They found that the ratio of crack growth rates at 100% relative humidity versus 0.05% relative humidity ranged from 7 to 10 at low ΔK values and tended to diminish to unity at very high ΔK values. Most importantly, they found that virtually all of the cracking rate acceleration occurred in the range from 0.15 to 1.5% relative humidity. Feeney, McMillan, and Wei (ref. 11) measured fatigue crack propagation rates in 2024-T3, 7075-T6, and 7178-T6 at very low ΔK levels in air at 90% and 10% relative humidity. Cracking rates in 7075-T6 and 7178-T6 were roughly two to three times higher at 90% relative humidity than at 10%. No change of cracking rate was observed in 2024-T3.

Bradshaw and Wheeler (refs. 10, 12) studied the effects of pure water vapor on fatigue crack propagation in DTD 5070A. They found that cracking rates were significantly affected by the level of water vapor pressure and that this effect was confined to a relatively narrow range of pressure which they called a transition zone; i.e., the variation of cracking rate with increasing water vapor pressure was sigmoidal. They defined the water vapor pressure at which significant cracking rate

acceleration begins as the critical pressure. With increasing ΔK from 6 to 12 $NM/m^{3/2}$, the critical pressure tended to increase, but the range of pressures over which transition occurred and the degree of cracking rate acceleration tended to decrease. In all cases transition was complete at water vapor pressures less than 130 Pa. Wei, et al. (ref. 47) reported a similar water vapor transition zone for fatigue crack propagation rates in 2219-T851. In this case transition occurred between 1 and 10 Pa water vapor pressure and did not vary significantly over a ΔK range from 10 to 20 $MN/m^{3/2}$.

Effect of frequency.- Intuitively, frequency would be expected to have an effect on fatigue crack propagation rates in a corrosive environment since chemical effects are generally time dependent; lower frequencies should produce higher da/dN values. However, intrinsic (i.e., due to the rate sensitivity of the material) frequency effects should be differentiated from those caused by the interaction of the material with the environment. Bradshaw and Wheeler (ref. 12) reported an intrinsic frequency effect in DTD 683, an Al-Zu-Mg-Cu alloy, from tests in hard vacuum. They did not find an intrinsic frequency effect in DTD 5070A, a clad Al-Cu-Mg alloy. In general, intrinsic frequency effects have not been reported for aluminum alloys.

Hartman, et al. (ref. 8) and Hartman and Schijve (ref. 9) studied the effect of frequencies ranging from 0.5 to 57 Hz on fatigue crack propagation rates in clad 2024-T3 and 7075-T6 in wet air (100% relative humidity) and dry air (0.05% relative humidity). For 2024-T3 they found that cracking rates at low ΔK values were accelerated as frequency was

lowered in both wet and dry air and that the effect became progressively smaller as ΔK became larger. The magnitude of the effect was much greater in dry air than in wet air; at low ΔK values in dry air, cracking rates at 0.5 Hz were more than ten times higher than at 57 Hz, but in wet air the difference was only a factor of two. Similar trends were observed for 7075-T6 except that in wet air little frequency effect was found at low ΔK values, and the maximum effect, about a factor of two between the frequency extremes, occurred at intermediate ΔK values. Wei (ref. 46) and Wei and Landes (ref. 48) tested 7075-T651 at 5 Hz and 143 Hz in dry argon (dew point ~ 133 K) and distilled water. They found that there was no frequency effect on fatigue crack propagation rates in dry argon and only a small effect in distilled water.

Bradshaw and Wheeler (ref. 12) investigated the effect of frequency on fatigue crack propagation rates in DTD 5070A in laboratory air and pure water vapor environments. They found little change in cracking rates in air at 1/60 Hz and 1 Hz, but rates at these frequencies were somewhat higher than rates measured at 100 Hz. In 2 kPa water vapor pressure they found that frequencies of 1 Hz and 100 Hz produced little overall difference in cracking rates. However, they found that frequency had a pronounced effect on the critical water vapor pressure where fatigue crack propagation rates accelerate markedly over the rates in hard vacuum. For a ΔK of 12 $MN/m^{3/2}$, the critical water vapor pressure at 100 Hz was approximately 65 Pa, which was two orders of magnitude higher than the critical pressure at 1 Hz.

Summarizing the effect of frequency, no effect is observed on fatigue crack propagation rates in inert environments such as hard vacuum or dry argon for most aluminum alloys. That is, most aluminum alloys are not intrinsically loading rate sensitive, and, therefore, observed frequency effects are environmentally induced. The effect of frequency is generally small in liquid water and at high water vapor pressure levels in gaseous environments. However, at intermediate levels of pure water vapor or in partially saturated gaseous environments, the frequency effect can be large in certain alloys and is a function of the water vapor pressure. Frequency strongly affects the critical water vapor pressure or transition zone where cracking rates begin to accelerate.

Mechanisms.- Over the years, many mechanisms have been proposed to account for the acceleration of aluminum alloy fatigue crack propagation rates by water vapor. These mechanisms generally fall into three categories: coldwelding, oxidation, and hydrogen embrittlement. Although coldwelding and oxidation mechanisms are now discounted, a discussion of them is included here for completeness.

Coldwelding is a joining phenomenon that occurs when clean metal surfaces bond together simply by the application of pressure. Wadsworth and Hutchings (ref. 5) proposed that the rapid coverage of freshly exposed surface by adsorbed gas molecules during fatigue cracking at higher gas pressures would prevent the coldwelding of surfaces that probably occurred under hard vacuum conditions. They suggested that prevention of coldwelding would produce higher fatigue crack growth

rates in gaseous environments than in hard vacuum. Freshly exposed aluminum surfaces produced by fatigue in hard vacuum should remain clean enough to promote coldwelding. Previously cracked surfaces contact each other (crack closure) during the unloading portion of a fatigue cycle even under positive stress ratios (ref. 49), and the compressive stresses in the crack wake are sufficient to cause reversed yielding (ref. 50). Under stresses of this magnitude, coldwelding of freshly exposed, clean aluminum surfaces produced by fatigue in hard vacuum may be promoted. Nevertheless, the prevention of coldwelding at higher gas pressures does not explain why water vapor greatly accelerates fatigue crack propatation and dry noble gases, dry air, and dry oxygen do not. Rapidly formed adsorbed gas layers or oxide films should prevent coldwelding in these dry gases. However, fatigue crack propagation rates in these dry gases at atmospheric pressure are roughly equivalent to the rates in hard vacuum.

Proposed oxidation mechanisms involve either the promotion of dislocation pileups or the elimination of slip reversal by oxide films. Shen, Podlaseck, and Kramer (ref. 42) suggested that fatigue crack propagation rates were higher in air than vacuum because of reduced dislocation mobility in air. They proposed that dislocation pileups occurred more easily in air due to the presence of an oxide film on the surface of the aluminum. Their proposal was based on dislocation theory and on the assumption that the oxide formed has a higher elastic modulus than the base metal. Dislocation theory indicates that dislocations in a lower modulus material approaching an interface with a higher modulus

material will be repelled and cause a dislocation pileup near the interface (ref. 51). Such pileups could restrict plastic deformation in the vicinity of the crack tip and accelerate fatigue crack propagation. However, investigations of the elastic properties of oxide films formed on aluminum surfaces by Grosskreutz (ref. 52) and Bradhurst and Leach (ref. 53) showed that these oxide films possess a lower, not higher, elastic modulus than the base aluminum. The oxide film would, therefore, tend to increase rather than decrease dislocation mobility.

Grosskreutz and Bowles (ref. 54) proposed that oxide films formed in air would inhibit reverse slip during load reversal in fatigue. As a consequence higher fatigue crack propagation rates would result from the accelerated formation of slip steps and dislocation dipoles. Conversely, fatigue crack propagation rates would be reduced in vacuum since reverse slip could occur more readily with no oxide film present and fewer slip steps and dislocation dipoles would be formed. However, this mechanism or any other oxidation mechanism seems to have little relevance to the role of water vapor when the bulk of the experimental evidence is considered. Even though dry oxygen oxidizes aluminum alloys readily, the presence of oxygen alone does not accelerate fatigue crack propagation except, perhaps, in nearly pure aluminum where the effect is small. On the other hand, aluminum alloy fatigue crack propagation rates are accelerated similarly in air, nitrogen, and oxygen whenever a critical partial pressure of water vapor is also present.

Broom and Nicholson (ref. 7) proposed that hydrogen embrittlement was the cause of shortened fatigue life in humid environments. They

speculated that adsorbed water vapor reacted with clean aluminum either at slip steps or at the crack tip to produce hydrogen ions which diffuse into the metal. They suggested that crack initiation would be assisted by the buildup of pressure in voids and that crack propagation rates could be accelerated by this pressure mechanism. Bradshaw and Wheeler (ref. 10) suggested that some form of hydrogen embrittlement mechanism was responsible for the acceleration of aluminum alloy fatigue crack propagation rates by water vapor. They showed that such a mechanism was compatible with the observed sigmoidal variation in cracking rates with water vapor pressure when the rate of diffusion of water vapor toward the advancing crack tip was taken into account. They further showed (ref. 12) that the variations in critical water vapor pressure and cracking rates with loading frequency supported a dynamic adsorption model. At a particular value of ΔK, critical cracking rate appeared to be proportional to the water vapor pressure divided by the frequency which suggested that the observed frequency effect was a result of the difference in time available for water vapor to react with freshly created surface of the advancing crack.

As a result of a study of environmental effects on fatigue crack propagation rates in 6.4 mm thick 7075-T651 over the temperature range from 295 to 380 K, Wei (ref. 46) also concluded that the acceleration of cracking rates by water vapor was caused by hydrogen embrittlement. He supported the contention that stress intensity was increased by a buildup of hydrogen pressure in the plastic zone ahead of the crack tip. He showed that fatigue crack growth in water, as well as in dry gaseous

environments, was controlled by thermally activated processes, with apparent activation energies that were strongly dependent on ΔK. From the comparison of apparent activation energies in water and dry gaseous environments he concluded that the mechanical process of creating new crack surface was the rate controlling process at low crack propagation rates (10^{-8}-10^{-7} m/cycle). He speculated that at higher cracking rates either the diffusion of water vapor to the crack tip or the diffusion and recombination of hydrogen ions in the region ahead of the crack tip might become the rate controlling process.

Direct evidence of hydrogen evolution during the fatigue of aluminum alloys in air was provided by Holshauser and Bennett (ref. 55). They found that hydrogen was evolved only in the most highly stressed region during bending and torsional fatigue of several aluminum alloys but that no gas was evolved during static bending or torsion even into the plastic range. Hydrogen evolution began before cracks were detectable when numerous slip bands were present on the surface, and the rate of hydrogen evolution increased when cracks were formed. No gas evolution was detected during fatigue at stresses too low to initiate cracking. They concluded that the source of hydrogen was a reaction between aluminum and water vapor in the air and not hydrogen previously contained in the metal. Montgrain and Swann (ref. 56) reported the release of hydrogen during sustained load intergrannular fracture of an Al-Zn-Mg alloy in vacuum after unstressed pre-exposure to air saturated with water vapor at room temperature. On the basis of the fractographic evidence and a comparison of results after pre-exposure to dry air and

moist air, they concluded that embrittlement had occurred as a result of grain boundary diffusion of hydrogen during pre-exposure in moist air and that hydrogen previously present in the metal played no significant role.

In the past aluminum alloys were not generally considered to be susceptible to hydrogen embrittlement, and suggestions that hydrogen played any significant role in the environmental cracking of aluminum alloys were considered dubious. To be certain, dry hydrogen gas has been shown to have little effect even at high pressure on the tensile properties (refs. 57, 58) of aluminum alloys or on their crack propagation rates under sustained loads (refs. 58 - 60) or fatigue loading (refs. 7, 10, 45, 46). However, research by Gest and Troiano (refs. 61, 62) demonstrated that 7075-T651 can be embrittled by cathodic charging with hydrogen. They showed that the embrittlement was reversible and varied with strain rate and temperature in a manner characteristic of hydrogen embrittlement in other materials. Considering a variety of experimental results, Spiedel (ref. 63) concluded unequivocally that hydrogen can reversibly embrittle aluminum alloys when its fugacity is high enough to drive diffusible hydrogen into the lattice. He also concluded that hydrogen embrittlement can cause both intergrannular and transgranular crack growth in aluminum alloys. Additional evidence of reversible aluminum alloy embrittlement by cathodic charging with hydrogen has been provided by Albrecht and his coworkers (refs. 64-66) and Jacko and Duquette (ref. 67) whose results

or 7075 in a variety of heat treatments confirm the earlier findings of Gest and Troiano (refs. 61, 62).

Any hydrogen embrittlement mechanism proposed to account for the acceleration of fatigue crack propagation by water vapor must necessarily involve a series of sequential or concurrent steps or processes which have been described by Marcus (ref. 68) for the general case of gas-metal interactions during fatigue. These processes are illustrated schematically in figure 3, which is based on an illustration in reference 69 for interactions between ferrous alloys and hydrogen bearing gases. Following gas phase transport to the crack tip region, molecular water must be physically adsorbed onto the surface. The next step, which is schematically called dissociative chemical adsorption, may involve all of the following processes: molecular chemical adsorption, dissociation of the adsorbed molecules, and atomic chemical adsorption. In any case the adsorbed water vapor reacts with the freshly produced aluminum crack surface to produce an oxide or hydrated oxide film and liberates atomic or ionic hydrogen. The hydrogen then enters the aluminum and is transported to the location where the embrittlement mechanism is operative. Transport of the hydrogen into the interior of the metal ahead of the crack tip may be caused by normal bulk diffusion, pipe diffusion through the dense dislocation network at the crack tip, and sweep in by mobile dislocations (ref. 27).

Wei, et al. (ref. 47) investigated fatigue crack propagation in 2219-T851 at various water vapor pressure levels and performed surface chemistry studies of the reaction of water vapor with clean 2219

surfaces. They correlated these results with a "pseudo static" one-dimensional model (ref. 70) of environment assisted fatigue crack growth which included both gas phase transport to the crack tip and surface reaction kinetics. They showed that acceleration of the cracking rate by water vapor was controlled by the rate of transport of water vapor to the crack tip rather than the aluminum water vapor reaction kinetics. A previous study of fatigue crack growth in 4340 steel exposed to water vapor by Pao, Wei, and Wei (ref. 71) had concluded that in this instance the cracking rate was limited by the surface reaction kinetics. Wei, et al. (ref. 47) attributed the contrasting results to an extremely large difference in the reaction rate constants for aluminum alloys and steel with water vapor. In both cases, however, they suggested that the acceleration of cracking rate by water vapor occurred as a result of hydrogen embrittlement.

The case for some form of hydrogen embrittlement as a mechanism to account for the acceleration of aluminum alloy fatigue crack propagation by water vapor is largely circumstantial. A specific hydrogen embrittlement mechanism in aluminum alloys remains unidentified. However, the dissociative reaction of water vapor with clean aluminum surfaces during fatigue provides a source of diffusible hydrogen, and the reversible embrittlement of 7075 aluminum by cathodic charging with hydrogen has been demonstrated. As opposed to the coldwelding and oxidation mechanisms, a hydrogen embrittlement mechanism is not at odds with the observed fatigue crack propagation behavior of aluminum alloys in a wide variety of gaseous environments.

MATERIAL, SPECIMENS, EQUIPMENT, AND PROCEDURE

Material and Specimens

The material used in this study was aluminum alloy 7475-T651 whose chemical composition, as reported by the manufacturer, is shown in Table 1. All specimens were cut from a single 25.4 mm thick plate of the alloy. Metallographic cross sections showing the microstructure of the plate are shown in figure 4. Longitudinal and transverse elastic modulus and mechanical properties were determined from tensile tests on standard 12.7 mm diameter tensile specimens. These data and the fracture properties of the plate reported by the manufacturer are shown in Table 2. Standard compact (CT) specimens were machined from the plate in LT and TL orientations for use in fatigue crack propagation experiments. The specimen configuration is shown in figure 5. Electric discharge machining was used to produce the sharp (radius $\leq$ 80 μm), straight through notch. Specimen thickness, B, was nominally 25 mm, and initial a/W ratios of 0.45 and 0.50 were used.

Environmental-Fatigue Testing System

Fatigue crack propagation experiments were performed in an environmental-fatigue testing system. Basically, the system consisted of an environmental chamber mounted on a servocontrolled, closed-loop hydraulically actuated testing machine. The environmental chamber enclosed the machine's specimen mounting apparatus including the specimen grips and the upper portions of the loading ram and load-reaction frame. Loads were transmitted to the upper portion of the ram

through a bellows in the chamber wall and were monitored by the output of a load cell located outside the chamber but in series with the specimen. This arrangement required that the load cell output be adjusted to account for the pressure differential inside and outside the chamber. The environmental chamber was a vertical stainless-steel cylinder with a horizontal parting plane in the middle for access. Either vacuum or controlled gaseous environments can be maintained within the chamber. A detailed description of the vacuum-pumping and pressure-control subsystems is given in reference 37.

Environmental Control and Monitoring

Experiments were performed at ambient temperature in three types of environments: (1) laboratory air; (2) a vacuum of 130 μPa; and (3) mixtures of water vapor and nitrogen at water vapor pressures ranging from 94 Pa to 3.8 kPa. For laboratory air tests the top half of the environmental chamber was lifted so that the specimen was exposed to the ambient laboratory environment. The water vapor level in laboratory air was not controlled or monitored, but relative humidity generally ranges from 40 to 80% in this laboratory.

For vacuum tests the chamber was initially evacuated to a pressure of 70 μPa. The pressure was then adjusted and maintained at 130 μPa by an automatic pressure control unit which admitted appropriate quantities of air while the chamber was continuously pumped. A quadrapole mass spectrometer residual gas analyzer was used to determine the composition of the vacuum environment. No significant contaminants were detected,

and the predominant component of the residual gas in the chamber was water vapor.

For the water vapor-nitrogen environments, the chamber was initially evacuated to a pressure of 130 μPa or less and was backfilled with a water vapor-nitrogen mixture immediately after stopping the pumps. The water vapor-nitrogen mixtures were obtained by bubbling high-purity nitrogen gas through a heated column of distilled water. Mass spectrometry and flame ionization gas chromatography showed that the nitrogen contained no significant contaminants and that the total hydrocarbon content as methane was less than one part per million. Total chamber pressures which would yield the desired water vapor partial pressures were determined by experiment. After filling the chamber to the appropriate total pressure, conditions within the chamber were allowed to stabilize for approximately one hour before beginning a fatigue experiment. Total pressure, dew point, and dry bulb temperature within the chamber were monitored continuously by an electronic manometer, a hygrometer, and a copper-constantan thermocouple, respectively.

Fatigue Testing Procedure

Fatigue crack propagation experiments were performed under constant amplitude loading at R = 0.2 under load control. Using a sinsusoidal waveform, tests were performed at frequencies of 1 Hz and 10 Hz. In most tests maximum and minimum loads were set to produce an initial stress intensity range, ΔK_o, of 8.8 $MN/m^{3/2}$. However, two tests were performed in vacuum with ΔK_o = 17.6 $MN/m^{3/2}$. Prior to carrying out

tests in vacuum and water vapor, specimens were fatigued in laboratory air to extend a starter crack about 1.3 mm from the notch tip. Subsequent testing was performed without interruption to avoid transient effects on crack propagation rate. To avoid notch geometry effects crack propagation data were ignored until a crack had extended at least 3 mm from the notch tip.

Due to the large displacements involved at long crack lengths, constant amplitude loading conditions could not be maintained in the latter portions of the tests. Maximum deviation from target ΔP was about 6% in the 1 Hz tests and 30% in the 10 Hz tests. Load-time records taken throughout each test were used for calculations of crack growth rates and stress intensity factors.

Crack Length, Crack Propagation Rate, and Stress Intensity Determinations

Effective crack lengths were determined continuously during fatigue testing by the compliance method. The crack-opening displacement at the crack mouth, V, was monitored by a clip gage mounted on the specimen's integral knife edges. The clip gage and load cell signals were fed to peak-reading digital voltmeters for determination of the maximum and minimum displacements and loads occurring during fatigue cycling. The output of the voltmeters was periodically recorded by a digital printer.

Values of the effective crack length were calculated from the compliance calibration equation

$$a/W = \sum_{j=0}^{3} b_j[\ln(EB\Delta V/\Delta P)]^j \qquad (7)$$

where $b_0 = -1.0429$, $b_1 = 0.5609$, $b_2 = -0.0470$, and $b_3 = 0.0008$. (Note that either V/P or $\Delta V/\Delta P$ may be used in this equation since the relationship between V and P is linear.) Equation (7) is based on a theoretical calculation of compliance of the CT specimen configuration by Newman (ref. 72). The basis for this equation and a comparison of theoretically and experimentally determined compliance is given in the Appendix.

Fatigue crack propagation rates were calculated by a secant averaging method. Conceptually, fatigue crack propagation rate is defined as the deriviative of the a versus N curve. However, a versus N data usually consist of discrete data points, and da/dN must be determined by an interpolation scheme. The crack propagation rates reported herein were calculated by averaging the secants between three sequential a,N data points. For the ith data point

$$da/dN = \frac{\frac{a_i - a_{i-1}}{N_i - N_{i-1}} + \frac{a_{i+1} - a_i}{N_{i+1} - N_i}}{2} \qquad (8)$$

Of course, da/dN was not calculated for either the first or last crack lengths.

Stress intensity factors were computed using the expression for the CT specimen configuration from reference 73

$$K = \frac{P}{BW^{1/2}} \left[\frac{2+\frac{a}{W}}{(1-\frac{a}{W})^{3/2}} \right] \left[0.866 + 4.64\frac{a}{W} - 13.32\frac{a^2}{W^2} + 14.72\frac{a^3}{W^3} - 5.6\frac{a^4}{W^4} \right] \quad (9)$$

Fractographic Characterization

Fracture surface morphology was characterized using scanning electron microscopy. Immediately after the broken specimens were removed from the environmental fatigue testing system, fracture surfaces were sprayed with a clear acrylic lacquer to prevent contamination. The lacquer was removed prior to microscopic examination by ultrasonic cleaning in acetone.

RESULTS AND DISCUSSION

Fatigue Crack Growth Behavior

The fatigue crack growth data obtained in this study were correlated using Paris' crack growth law, equation (3). Data from replicate tests were correlated as a single set. Values of the empirical constants C and n were determined for each test condition by fitting the equation to the data by the method of least squares. As noted previously, significant deviations from constant amplitude loading conditions occurred at long crack lengths. To avoid any effects of these loading errors, the correlations were limited to data for crack lengths where the loading errors were small. A load deviation of 1% of target ΔP was allowed in correlations of 1 Hz data, and a 5% deviation was allowed in correlations of 10 Hz data. Values of C and n for each test condition are listed in table 3. As can be seen in many of the figures that follow, equation (3) fits the data well at low to moderate values of ΔK.

Vacuum.- Figure 6 shows the variation of da/dN with ΔK for the TL orientation in a vacuum of 130 μPa at frequencies of 1 Hz and 10 Hz. A similar plot of the variation of da/dN with ΔK for the LT orientation under the same vacuum and frequency conditions is shown in figure 7. No discernible difference in the cracking rates at the two frequencies was observed for either orientation.

The variation of da/dN with ΔK for the two orientations is compared in figures 8 and 9 for frequencies of 1 Hz and 10 Hz, respectively. Cracking rates for the two orientations were nearly identical

at low ΔK values. Although cracking rates for the TL orientation were somewhat higher than those for the LT orientation at high ΔK values, little difference in the cracking rates was observed except at ΔK values in excess of 20 $MN/m^{3/2}$. Since the fatigue response for the two orientations was generally similar in vacuum, only the LT orientation was used in the experiments in other environments.

Laboratory air.- Figure 10 shows the variation of da/dN with ΔK in laboratory air at frequencies of 1 Hz and 10 Hz. The ratio of the cracking rate at 1 Hz to that at 10 Hz was about 1.4 at low ΔK values and increased to about a factor of 2 at high ΔK values. Since the ambient laboratory environment was purposely uncontrolled, a large change in water vapor partial pressure in the air was likely from one test to the other. The 1 Hz and 10 Hz tests were performed during different seasons of the year. Prevailing relative humidity is significantly higher in the season when the 1 Hz test was performed than in the season when the 10 Hz test was performed. As a consequence the difference in the cracking rates observed in these tests is more likely the result of environmental variations rather than the change in frequency. The variation of da/dn with ΔK in laboratory air is compared to that in vacuum in figures 11 and 12 for frequencies of 1 Hz and 10 Hz, respectively. At 1 Hz the cracking rate in laboratory air was about 3.5 times higher than the cracking rate in vacuum over the entire range of ΔK values. However, at 10 Hz the ratio of the cracking rate in laboratory air to that in vacuum decreased from about a factor of 3 at low ΔK values to about a factor of 2 at high ΔK values.

Water vapor.- The variation of da/dN with ΔK for various water vapor pressures at frequencies of 1 Hz and 10 Hz is presented in figures 13-18. These water vapor pressures range from 94 Pa to 3.8 kPa and correspond to relative humidities ranging from about 4% at 22°C to about 100% at 28°C. On the whole, these results indicate that the effect of frequency on fatigue crack growth rates at these water vapor pressures was insignificant. Figure 19 shows the variation of da/dN with ΔK for various water vapor pressures and in vacuum at a frequency of 1 Hz. At low ΔK values cracking rates at the lowest and highest water vapor pressures were, respectively, about two times higher and five times higher than the cracking rates in vacuum. At high ΔK values cracking rates at the lower water vapor pressures tended to converge with rates in vacuum, but cracking rates at the higher water vapor pressures remained substantially higher than the rates in vacuum. As can be seen in figure 20, the general trends in the fatigue crack behavior at 10 Hz were similar to the trends observed at 1 Hz.

The variation of da/dN with water vapor pressure at four ΔK levels is shown in figure 21. Crack growth data obtained in hard vacuum are plotted as if the total pressure were due to water vapor only. The effect of water vapor on fatigue crack growth rates was qualitatively similar at each ΔK level. Even at the lowest water vapor pressure used in these tests, a relatively dry condition, a significant effect of water vapor on cracking rates was observed. Little change in the cracking rates occurred over the water vapor pressure range from 94 Pa

to 1.03 kPa. However, an abrupt acceleration in cracking rates was observed at higher water vapor pressures.

These results suggest that corrosion fatigue of 7475-T651 in water vapor is not a simple interaction of mechanical fatigue and stress corrosion cracking but is more likely the result of a more complex phenomenon. Although fatigue crack growth rates were as much as five times higher in water vapor than in hard vacuum, rates in water vapor were unaffected by a ten fold change in frequency. If the acceleration of fatigue crack growth rates in water vapor were a result of stress corrosion cracking, fatigue crack growth rates should have been higher at 1 Hz than 10 Hz. However, additional experiments over a wider range of frequencies would be necessary to determine fully whether stress corrosion cracking affects the corrosion fatigue of 7475-T651 in water vapor.

Bradshaw and Wheeler (ref. 12) studied the effect of pure water vapor on fatigue crack growth in 1.6 mm thick specimens of aluminum alloy DTD 5070A. Wei et al. (ref. 47) performed a similar study using 16.5 mm thick specimens of aluminum alloy 2219-T851. The present results for 7475-T651, an Al-Zn-Mg-Cu alloy, are compared to the results for DTD 5070A in figure 22 and to the results for 2219-T851 in figure 23. For DTD 5070A and 2219-T851, both of which are Al-Cu-Mg alloys, cracking rates were virtually unaffected by water vapor until a threshold pressure was reached. Cracking rates then increased rapidly but reached a maximum value at a pressure only one order of magnitude higher than the threshold pressure. For DTD 5070A this transition in

cracking rates was found to be sensitive to a change of frequency; a 100 fold increase in frequency produced a two orders of magnitude increase in the threshold water vapor pressure. While the present results for 7475-T651 indicate that a cracking rate transition occurs at water vapor pressures less than 94 Pa, a second, frequency-insensitive transition in cracking rates was observed at high water vapor pressures. This second transition in cracking rates for 7475-T651 occurred at water vapor pressures in excess of the highest pressures at which DTD 5070A and 2219-T851 were tested.

Fractographic Characterization

Fracture surfaces of specimens fatigued in hard vacuum and at various water vapor pressures were characterized in an attempt to correlate fracture morphology with environmental interaction. Macroscopically, the fracture morphology of specimens tested in vacuum contrasted sharply with that of specimens tested in water vapor. As illustrated in figure 24, the fracture morphology of specimens tested in vacuum varied across the thickness of the specimens. Compared to the mid-thickness region, the fracture surface near the edges was highly roughened or rumpled. With increasing ΔK the roughened portions of the fracture surface grew toward the center. This change in morphology from the center to the edges indicates a change in fatigue crack propagation mode associated with a change of stress state along the crack front. In the mid-thickness region where the fracture plane was normal to the applied load axis, the crack propagated predominantly in the

opening (tensile) mode. However, the highly roughened surface indicates that the crack propagated in a mixed opening/sliding (tensile/shear) mode in the near-edge regions.

Figure 25 shows optical macrographs of specimens tested at low and high water vapor pressures. Compared to specimens tested in vacuum, these specimens exhibited a more uniform fracture morphology across the thickness. Although some roughening of the near-edge regions was exhibited by specimens tested at low water vapor pressure (See fig. 25(a).), the process began at higher ΔK values and involved much less of the fracture surface. Little evidence of fracture surface roughening was found on specimens tested at high water vapor pressures (See fig. 25(b).), but crack front curvature was noticeable at high ΔK values.

Differences in the amount of residual deformation on the fracture surfaces of specimens tested in water vapor and vacuum may be evidence of an environmental interaction with the plastic zone ahead of the crack tip. Reduced deformation on the fracture surfaces of the specimens tested in water vapor may be the result of plastic zone embrittlement. The greater deformation on the fracture surfaces of specimens tested in vacuum may have caused crack closure at higher loads which might account for the differences in fatigue crack growth rates in vacuum and water vapor.

At relatively low magnification in the scanning electron microscope, the fracture morphology of specimens tested in water vapor was generally similar to that of specimens tested in vacuum. As shown in figure 26, the most prominent features at low ΔK values were fatigue

plateaus and tear ridges. At high ΔK values (See fig. 27.) fatigue plateaus were less prevalent. The fracture surfaces were more highly deformed, and large secondary cracks were common. Small patches of fine dimpled rupture were found at higher magnification as shown in figure 28.

Fatigue striations were found on the fracture surfaces of specimens tested in water vapor and vacuum. However, as shown in figure 29, their appearance was quite different. Fatigue striations formed in water vapor were classic in appearance, but striations formed in vacuum were poorly defined and much less prevalent on the fracture surface. Striation spacings were compared to fatigue crack growth rates. In general, good agreement was found for specimens tested in water vapor, but discrepancies were large for specimens tested in vacuum.

In addition to fatigue striations, numerous areas of transverse cracking were found at low to moderate ΔK values on specimens tested in vacuum. Examples are shown in figure 30. These cracks were parallel and fairly regularly spaced. Fine striation-like markings were found on the relatively flat surfaces between the cracks. Although some transverse cracks were also found on specimens tested in water vapor, this feature was much more prevalent on specimens tested in vacuum. The much lower amount of transverse cracking exhibited by specimens tested in water vapor may be additional evidence of plastic zone embrittlement.

Mechanisms

The enhancement of aluminum alloy fatigue crack growth rates by water vapor has been attributed to a mechanism of hydrogen embrittlement (refs. 7, 10, 46, 47). Such a mechanism involves a series of sequential or concurrent steps or processes which can be schematically outlined. Following the diffusion of water vapor to the crack tip vicinity, molecular water is adsorbed on the clean aluminum surface produced by the advancing crack. The reaction of water with aluminum produces an oxide or hydrated oxide film and liberates hydrogen. After dissociation to the atomic or ionic form, hydrogen adsorbs on the aluminum surface and is transported into the plastic zone ahead of the crack tip where localized embrittlement occurs. Hydrogen transport within the plastic zone is presumed to occur by mobile dislocation sweep-in in addition to normal bulk diffusion.

If hydrogen embrittlement is the causative mechanism, fatigue crack growth rates in water vapor would depend on the kinetics associated with the processes outlined above. The results of Bradshaw and Wheeler (ref. 12) and Wei et al. (ref. 47) for two Al-Cu-Mg alloys showed a cracking rate transition which occurred at relatively low water vapor pressures. While the present results for 7475-T651 indicate that a similar transition occurs at low water vapor pressures, a second transition in cracking rates was observed at high water vapor pressures. If both of these cracking rate transitions are to be accommodated by a hydrogen embrittlement mechanism, the rate controlling

process at high water vapor pressures must be different from the rate controlling process at low water vapor pressures.

Although the fractographic evidence presented herein tends to support plastic zone embrittlement, the transition in cracking rates observed at high water vapor pressures may be due to some other mechanism such as anodic dissolution. Since the relative humidity levels during the tests at high water vapor pressures were at or near 100%, water reaching the crack tip may have been liquid rather than vapor. Such conditions may be favorable for the onset of an anodic dissolution mechanism. Some insight regarding mechanisms may be gained from fatigue crack growth tests where the potential of the specimen is controlled with respect to the test environment.

CONCLUDING REMARKS

An investigation has been performed to assess the effects of water vapor on fatigue crack growth in 7475-T651 aluminum alloy plate and to determine whether these effects are frequency dependent. Twenty-five mm thick compact specimens were subjected to constant amplitude fatigue testing at a load ratio of 0.2. Fatigue crack growth rates were determined at frequencies of 1 Hz and 10 Hz in hard vacuum and laboratory air and in mixtures of water vapor and nitrogen at water vapor partial pressures ranging from 94 Pa to 3.8 kPa. Fracture surfaces were characterized in an attempt to correlate fracture morphology with environmental interaction.

Both the TL and LT orientations were tested in hard vacuum. Little difference in the cracking rates for the two orientations was observed except at high stress intensity factor ranges where rates for the TL orientation were somewhat higher than those for the LT orientation. No discernible difference in the cracking rates at the two frequencies was observed for either orientation. Only the LT orientation was used for tests in other environments.

In laboratory air cracking rates were higher at 1 Hz than 10 Hz. The largest difference in the cracking rates at the two frequencies was observed at high stress intensity factor ranges. At 1 Hz cracking rates in laboratory air were about 3.5 times higher than those in vacuum at both low and high stress intensity factor ranges. At 10 Hz the ratio of the cracking rates in laboratory air to those in vacuum decreased from about a factor of 3 at low stress intensity factor ranges

to about a factor of 2 at high stress intensity factor ranges.

At the lowest water vapor pressure tested, 94 Pa, a significant effect of water vapor on cracking rates was observed. At low stress intensity factor ranges cracking rates at this pressure were two times higher than rates in vacuum. Over the water vapor pressure range from 94 Pa to 1.03 kPa, little change in the cracking rates occurred. However, an abrupt acceleration in the cracking rates was observed at water vapor pressures in excess of 1.03 kPa. At low stress intensity factor ranges cracking rates at the highest water vapor pressure tested were five times higher than rates in vacuum. These results indicate that one transition in cracking rates occurred at low water vapor pressures and another transition occurred at high water vapor pressures. The abrupt acceleration of fatigue crack growth rates observed at high water vapor pressures suggests either a change in the rate controlling kinetics or a change in the basic mechanism as a function of pressure.

The effect of frequency on fatigue crack growth rates was insignificant over the entire water vapor pressure range tested. This result suggests that corrosion fatigue of 7475-T651 in water vapor is not a simple interaction of mechanical fatigue and stress corrosion cracking but is more likely the result of a more complex phenomenon.

Fracture surfaces of specimens tested in water vapor exhibited less residual deformation than the fracture surfaces of specimens tested in vacuum. This difference in the amount of deformation may be evidence of an environmental interaction with the plastic zone ahead of the crack tip. Reduced deformation on the fracture surfaces of speci-

mens tested in water vapor may be the result of plastic zone embrittlement. Greater deformation on the fracture surfaces of specimens tested in vacuum may have caused crack closure at higher loads which might account for the differences in fatigue crack growth rates in vacuum and water vapor.

APPENDIX

COMPLIANCE CALIBRATION

The method of crack length determination used in this study was based on a calibration of specimen compliance. Inherently, this method is based on the assumption that the behavior of the specimen is elastic. Accordingly, for the compact (CT) specimen configuration (See fig. 5.)

$$EBV/P = F(a/W) \qquad (A1)$$

As a part of this study, CT specimen compliance was determined experimentally and compared to theoretically calculated values.

The experimental compliance of the CT specimen configuration was determined by measuring the crack-opening displacement as a function of load at various values of a/W. A single CT specimen of 7475-T651 in the TL orientation was used for these experiments. A thin (approximately 320 μm) slot was machined through the specimen thickness from the tip of the notch in a plane perpendicular to the load line and was extended by incremental cutting. The length of the slot was measured on each face of the specimen using a tool maker's microscope. A clip gage was used to measure the crack-opening displacement at the crack mouth at discrete values of load while the specimen was loaded in tension. In each succeeding test at a longer slot length, the maximum load was adjusted downward to maintain a constant, very small plastic zone size. Values of V/P were determined from the slope of straight lines fitted to the load-displacement data using the method of least squares. The

measured elastic modulus of the material was used to calculate EBV/P. Values of a/W and EBV/P from these experiments are shown in table A1.

Theoretical compliance values for the CT specimen configuration have been obtained by Newman (ref. 72). His analysis employed the method of boundary collocation and included the effects of finite boundaries and pin-loaded holes. He reported compliance values for plane-stress conditions with Poisson's ratio equal to 0.3 for a/W ratios ranging from 0.2 to 0.8. His calculations showed good agreement with experimental data on two aluminum alloys at a/W ratios ranging from 0.35 to 0.6. The theoretical compliance values reported by Newman are shown in table A2.

Figure A1 shows the experimental (from this study) and theoretical values of compliance for the CT specimen configuration as a function of a/W. The theoretical and experimental values are in excellent agreement over the entire range of the experimental data. A compliance calibration equation was developed by fitting a polynomial expression to the theoretical data using the method of least squares. The polynomial expression is

$$a/W = \sum_{j=0}^{3} b_j[\ln(EBV/P)]^j \qquad (A2)$$

where $b_0 = -1.0429$, $b_1 = 0.5609$, $b_2 = -0.0470$, and $b_3 = 0.0008$. A comparison between the polynomial expression and the theoretical values is shown in figure A2. Values of a/W computed using the polynomial

expression were within $\pm$ 0.4% of the theoretical values for $0.2 \leq a/W \leq 0.8$.

TABLE A1.- EXPERIMENTAL COMPLIANCE FOR 7475-T651 ALUMINUM ALLOY CT SPECIMEN

a/W	EBV/P
0.503	55.99
.520	59.86
.543	68.56
.567	75.19
.593	85.35
.618	98.52
.638	111.3
.657	121.5
.679	144.7
.689	155.0
.698	161.2
.708	173.9
.717	188.7
.728	206.5
.738	223.2
.747	240.5
.758	263.6
.767	288.2
.777	316.5
.788	348.1
.798	388.2
.808	427.3

TABLE A2.- THEORETICAL COMPLIANCE FOR CT SPECIMEN CONFIGURATION FROM REFERENCE 72 (PLANE STRESS CONDITIONS, $\nu = 0.3$)

a/W	EBV/P
0.20	17.69
.25	20.91
.30	24.90
.35	29.89
.40	36.18
.45	44.23
.50	54.76
.55	69.00
.60	89.04
.65	118.7
.70	165.5
.75	245.4
.90	397.0

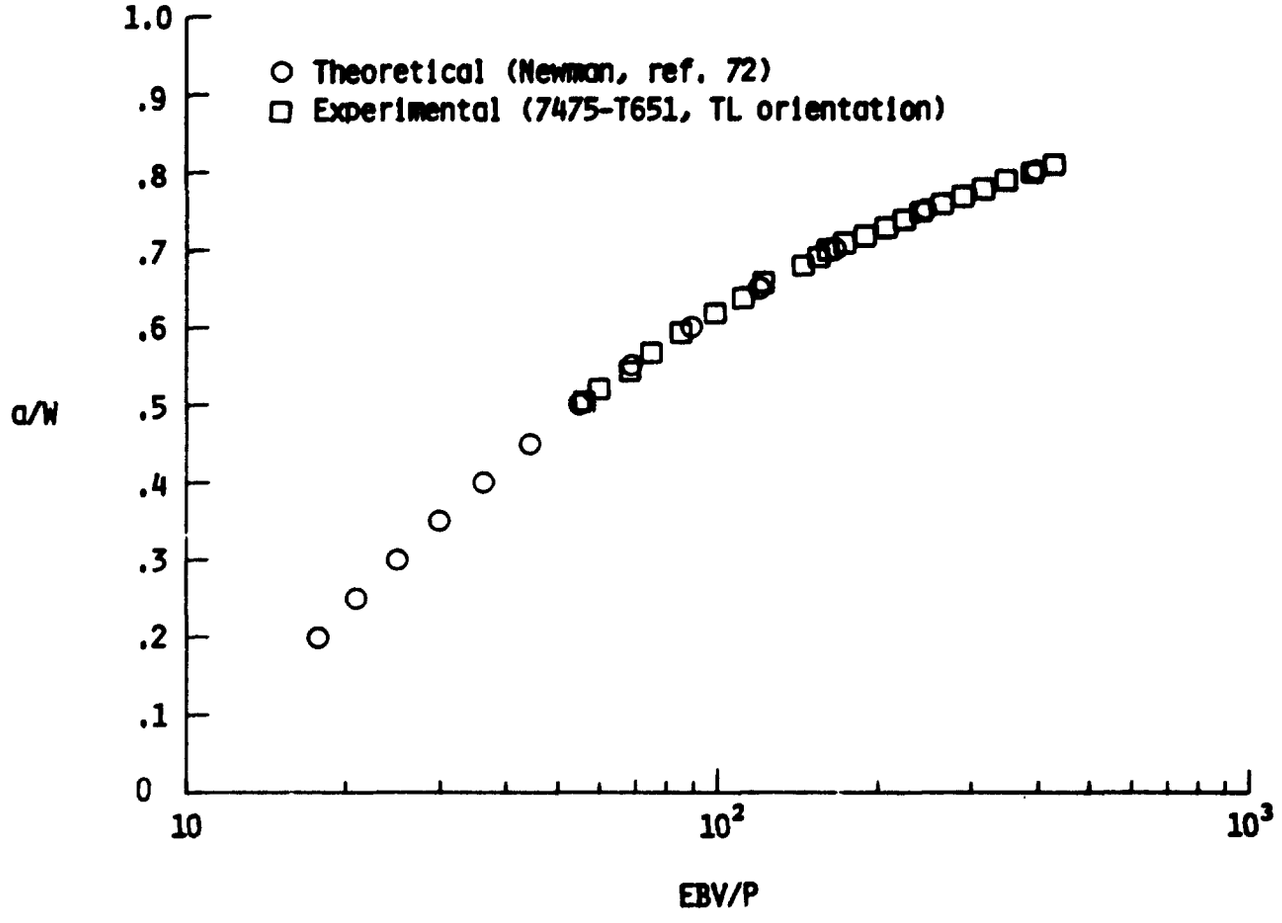

Figure A1. - Comparison of experimental and theoretical compliance for the CT specimen configuration.

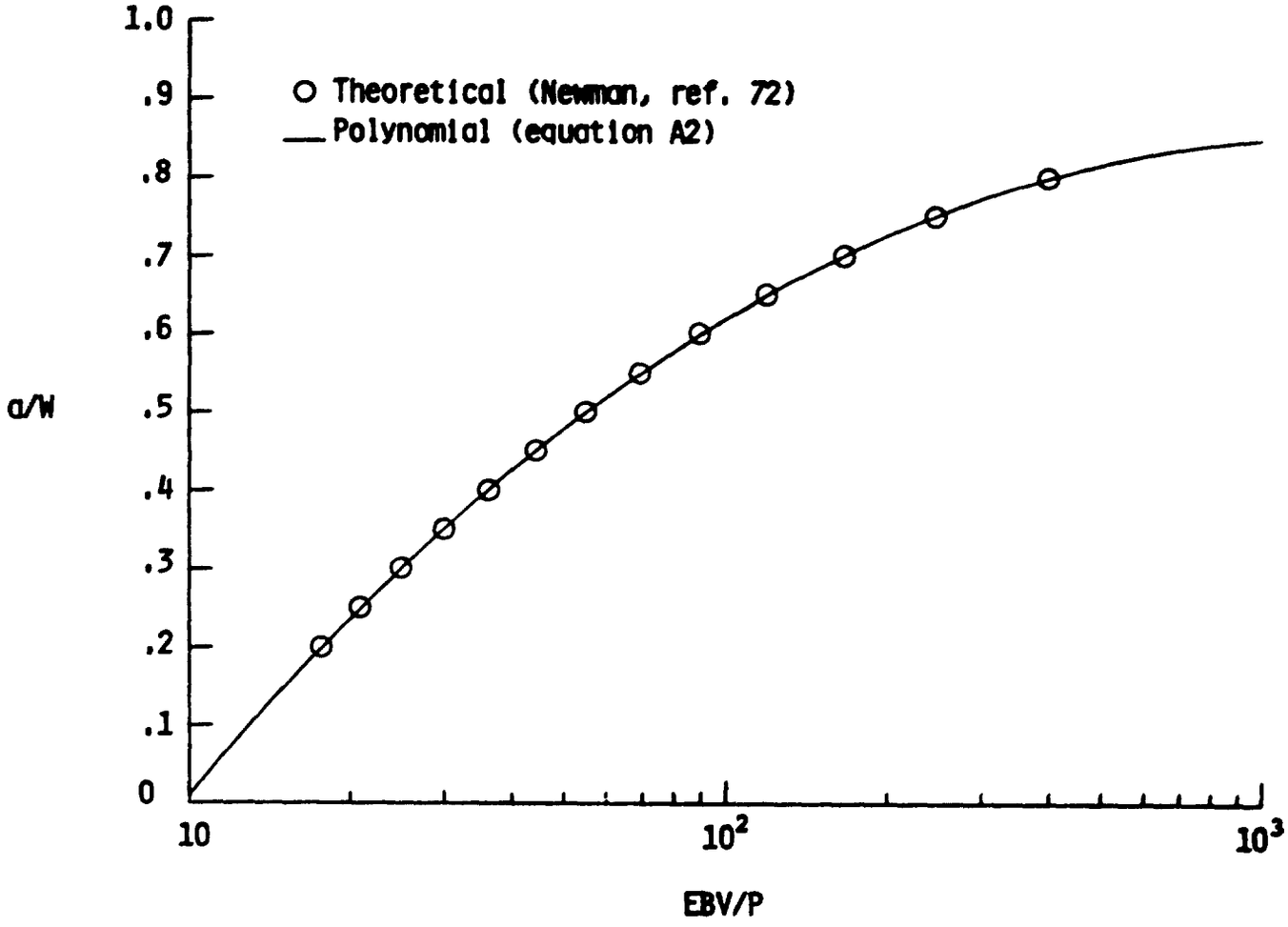

Figure A2. - Comparison of theoretical compliance for the CT specimen configuration with a fitted polynomial.

REFERENCES

1. Vlieger, H.: Application of Fracture Mechanics in Designing Built-Up Sheet Structure. Fracture Mechanics Design Methodology. AGARD-CP-221, 1977, pp. 5-1 -- 5-18.

2. Cooper, Thomas D.; and Kelto, Clifford A.: Fatigue in Machines and Structures - Aircraft. Fatigue and Microstructure, American Society for Metals, 1979, pp. 29-56.

3. Coffin, M. D.; and Tiffany, C. F.: New Air Force Requirements for Structural Safety, Durability, and Life Management. J. Aircraft, vol. 13, no. 2, Feb. 1976, pp. 93-98.

4. Gough, H. J.; and Sopwith, D. G.: Atmospheric Action as a Factor in Fatigue of Metals. J. Inst. Metals, vol. 49, 1932, pp. 93-112.

5. Wadsworth, N. J.; and Hutchings, J.: The Effect of Atmospheric Corrosion on Metal Fatigue. Phil. Mag., vol. 3, no. 34, Oct. 1958, pp. 1154-1166.

6. Wadsworth, N. J.: The Effect of Environment on Metal Fatigue. Internal Stresses and Fatigue in Metals, Gerald M. Rassweiler and William L. Grube, eds., Elsevier Publishing Co., 1959, pp. 382-396.

7. Broom, Trevor; and Nicholson, Anthony: Atmospheric Corrosion - Fatigue of Age - Hardened Aluminum Alloys. J. Inst. Metals, vol. 89, 1961, pp. 183-190.

8. Hartman, A.; Jacobs, F. A.; Nederveen, A.; and De Rijk, P.: Some Tests on the Effect of Environment on the Propagation of Fatigue Cracks in Aluminum Alloys. NLR TN M. 2182, Nat. Aerosp. Lab. (The Netherlands), 1967.

9. Hartman, A.; and Schijve, J.: The Effects of Environment and Load Frequency on the Crack Propagation Law for Macro Fatigue Crack Growth in Aluminum Alloys. NLR MP 68001 U, Nat. Aerosp. Lab. (The Netherlands), 1968.

10. Bradshaw, F. J.; and Wheeler, C.: The Effect of Environment on Fatigue Crack Growth in Aluminum and Some Aluminum Alloys. Appl. Matls. Res., vol. 5, Apr. 1966, pp. 112-160.

11. Feeney, J. A.; McMillan, J. C.; and Wei, R. P.: Environmental Fatigue Crack Propagation of Aluminum Alloys at Low Stress Intensity Levels. Boeing Co. Report D6-60114, 1969.

12. Bradshaw, F. J.; and Wheeler, C.: The Influence of Gaseous Environment and Fatigue Frequency on the Growth of Fatigue Cracks in Some Aluminum Alloys. Int. J. Frac. Mech., vol. 5, no. 4, Dec. 1969, pp. 255-268.

13. Forsyth, P. J. E.: A Two Stage Process of Fatigue Crack Growth. Proceedings of the Crack Propagation Symposium (Cranfield), vol. 1, Sept. 1961, pp. 76-94.

14. Laird, C.; and Smith, G. C.: Initial Stages of Damage in High Stress Fatigue in Some Pure Metals. Phil. Mag., vol. 8, no. 95, Nov. 1963, pp. 1945-1963.

15. Forsyth, P. J. E.: Fatigue Damage and Crack Growth in Aluminum Alloys. Acta Met., vol. 11, no. 7, July 1963, pp. 703-715.

16. Griffith, A. A.: The Phenomenon of Rupture and Flow in Solids. Phil. Trans. of the Royal Soc. of London, vol. 221A, 1920, pp. 163-198.

17. Irwin, G. R.: Analysis of Stresses and Strains Near the End of a Crack Traversing a Plate. J. Appl. Mech., vol. 24, no. 3, Sept. 1957, pp. 361-364.

18. Williams, M. L.: On the Stress Distribution at the Base of a Stationary Crack. J. Appl. Mech., vol. 24, no. 1, Mar. 1957, pp. 109-114.

19. Newman, J. C., Jr.: Finite Element Analysis of Fatigue Crack Propagation--Including the Effects of Crack Closure. Ph.D. Thesis, Virginia Polytech. Inst. & State Univ., 1974.

20. Paris, P. C.; Gomez, M. P.; and Anderson, W. E.: A Rational Analytic Theory of Fatigue. The Trend in Engineering, U. of Wash., Seattle, vol. 13, no. 1, Jan. 1961, p. 9.

21. Paris, P. C.; and Erdogan, F.: A Critical Analysis of Crack Propagation Laws. J. Basic Engr., Trans. ASME, vol. 85, Series D, no. 4, Dec. 1963, pp. 528-534.

22. Paris, P. C.: The Fracture Mechanics Approach to Fatigue. Fatigue - An Interdisciplinary Approach, Syracuse U. Press, 1964, pp. 107-132.

23. Hudson, C. Michael; and Scardina, J. T.: Effect of Stress Ratio on Fatigue Crack Growth in 7075-T6 Aluminum-Alloy Sheet. Engr. Frac. Mech. J., vol. 1, no. 3, 1969.

24. Forman, R. G.; Kearney, V. E.; and Engle, R. M.: Numerical Analysis of Crack Propagation in Cyclic Loaded Structure. J. Basic Engr., Trans. ASME, vol. 89, Series D, no. 3, 1967, pp. 459-464.

25. Erdogan, Fazil: Crack Propagation Theories. Fracture, Volume II, H. Liebowitz, ed., Acad. Press, 1968, pp. 497-590.

26. Hudson, C. Michael: Effect of Stress Ratio on Fatigue Crack Growth in 7075-T6 and 2024-T3 Aluminum-Alloy Sheet Specimens. NASA TN D-5390, 1969.

27. Marcus, H. L.: Environmental Effects II: Fatigue Crack Growth in Metals and Alloys. Fatigue and Microstructure, ASM, 1979, pp. 365-383.

28. Staehle, R. W.: A Point of View Concerning Mechanisms of Environment-Sensitive Cracking of Engineering Materials. Mechanisms of Environment Sensitive Cracking of Materials, P. R. Swann, F. P. Ford, A. R. C. Westwood, eds., The Metals Soc., 1977, pp. 574-602.

29. Speidel, M. O.; Blackburn, M. J.; Beck, T. R.; and Feeney, J. A.: Corrosion Fatigue and Stress Corrosion Crack Growth in High Strength Aluminum Alloys, Magnesium Alloys, and Titanium Alloys Exposed to Aqueous Solutions. Corrosion Fatigue: Chemistry, Mechanics, and Microstructure, O. Devereux, A. J. McEvily, R. W. Staehle, eds., NACE, 1972, pp. 324-345.

30. Gallagher, J. P.: Corrosion Fatigue Crack Growth Behavior Above and Below K_{ISCC}. NRL Rpt. 7064, 1970.

31. Barsom, J. M.: Corrosion Fatigue Crack Propagation Below K_{ISCC}. J. Engr. Fract. Mech., vol. 3, no. 1, July 1971.

32. Wei, R. P.; and Landes, J. D.: Correlation Between Sustained-Load and Fatigue Crack Growth in High-Strength Steels. Materials Research and Standards, vol. 9, no. 7, July 1969, pp. 25-27, 44, 46.

33. Gerberich, W. W.; Birat, J. P.; and Zackay, V. F.: On the Superposition Model for Environmentally Assisted Fatigue Crack Propagation. Corrosion Fatigue: Chemistry, Mechanics, and Microstructure, O. Devereux, A. J. McEvily, R. W. Staehle, eds., NACE, 1972, pp. 396-408.

34. Wei, R. P.: Some Aspects of Environment-Enhanced Fatigue-Crack Growth. Engr. Frac. Mech., vol. 1, 1970, pp. 633-651.

35. McEvily, A. J.; and Wei, R. P.: Fracture Mechanics and Corrosion Fatigue. Corrosion Fatigue: Chemistry, Mechanics, and Microstructure, O. Devereux, A. J. McEvily, R. W. Staehle, eds., NACE, 1972, pp. 381-395.

36. Duquette, D. J.: Environmental Effects I: General Fatigue Resistance and Crack Nucleation in Metals and Alloys. Fatigue and Microstructure, ASM, 1979, pp. 335-363.

37. Hudson, C. Michael: A Study of Fatigue and Fracture in 7075-T6 Aluminum Alloy in Vacuum and Air Environments. NASA TN D-7262, 1973.

38. Snowden, K. U.: Effect of Air Pressure on the Fatigue of Lead and Aluminum. Nature, vol. 189 (475B), 1961, pp. 53-54.

39. Christensen, R. H.: Fatigue Cracking of Metals Accelerated by Prolonged Exposure to High Vacuum. Douglas Aircraft Co., Missile and Space Systems Div., Eng. Paper No. 1636, 1963.

40. Ham, John L.; and Reichenbach, George S.: Fatigue Testing of Aluminum in Vacuum. Symposium on Materials for Aircraft, Missiles and Space Vehicles, ASTM STP 345, 1963, pp. 3-13.

41. Hordon, M. J.: Fatigue Behavior of Aluminum in Vacuum. Acta Met., vol. 14, Oct. 1966, pp. 1173-1178.

42. Shen, H.; Podlaseck, S. E.; and Kramer, I. R.: Effects of Vacuum on the Fatigue Life of Aluminum. Acta Met., vol. 14, no. 3, 1966, pp. 341-346.

43. Shen, Harold: Effect of Vacuum Environment on the Mechanical Behavior of Materials Martin Co., MCR 67-423, 1967.

44. Wright, M. A.; and Hordon, M. J.: Effect of Residual Gas Composition on the Fatigue Behavior of Aluminum. Trans. Met. Soc. AIME, vol. 242, Apr. 1968, pp. 713-714.

45. Hartman, A.: On the Effect of Oxygen and Water Vapor on the Propagation of Fatigue Cracks in 2024-T3 Alclad Sheet. Int. J. Frac. Mech., vol. 1, no. 3, Sept. 1965, pp. 167-188.

46. Wei, R. P.: Fatigue-Crack Propagation in a High-Strength Aluminum Alloy. Int. J. Frac. Mech., vol. 4, no. 2, June 1968, pp. 159-170.

47. Wei, R. P.; Pao, P. S.; Hart, R. G.; Weir, T. W.; and Simmons, G. W.: Fracture Mechanics and Surface Chemistry Studies of Fatigue Crack Growth in an Aluminum Alloy. Met. Trans. A, vol. 11 A, Jan. 1980, pp. 151-158.

48. Wei, R. P.; and Landes, J. D.: The Effect of D_2O on Fatigue-Crack Propagation in a High-Strength Aluminum Alloy. Int. J. Frac. Mech., vol. 5, no. 1, Mar. 1969, pp. 69-71.

49. Elber, Wolf: The Significance of Fatigue Crack Closure. Damage Tolerance in Aircraft Structures, ASTM STP 486, 1970, pp. 230-242.

50. Newman, J. C., Jr.: A Finite-Element Analysis of Fatigue Crack Closure. Mechanics of Crack Growth, ASTM STP 590, 1976, pp. 281-301.

51. Weertman, Johannes; and Weertman, Julia R.: Elementary Dislocation Theory, The Macmillan Co., 1964, p. 170-173.

52. Grosskreutz, J. C.: The Effects of Oxide Films on Dislocation-Surface Interactions in Aluminum. Surf. Sci., vol. 8, 1967, pp. 173-190.

53. Bradhurst, D. H.; and Leach, J. S. Llewelyn: The Mechanical Properties of Anodic Films on Aluminum. Trans. Brit. Cer. Soc., vol. 62, no. 9, Sept. 1963, pp. 793-806.

54. Grosskreutz, J. C.; and Bowles, C. Q.: Effect of Environmental Gases on the Surface Deformation of Aluminum and Gold in Fatigue. Environment-Sensitive Mechanical Behavior, A.R.C. Westwood and N.S. Stoloff, eds., Met. Soc. Conferences, vol. 35, Gordon and Breach Science Publishers, 1966, pp. 67-105.

55. Holshauser, W. L.; and Bennett, J. A.: Gas Evolution From Metal Surfaces During Fatigue Stressing. Proc. ASTM, vol. 62, 1962, pp. 683-694.

56. Montgrain, L.; and Swann, P. R.: Electron Microscopy of Hydrogen Embrittlement in a High Purity Al-Zn-Mg Alloy. Hydrogen in Metals, I. M. Bernstein and Anthony W. Thompson, eds., ASM, 1974, pp. 575-584.

57. Chandler, W. T.; and Walter, R. J.: Effects of High Pressure Hydrogen on Metals at Ambient Temperature. NASA CR-10245, 1969.

58. Speidel, M. O.; and Hyatt, M. V.: Stress Corrosion Cracking of High Strength Aluminum Alloys. Advances in Corrosion Science and Technology, vol. 2, Mars G. Fontana and Roger W. Staehle, eds., Plenum Press, 1972, pp. 115-335.

59. Lorenz, P. M.: Effect of Pressurized Hydrogen upon Inconel 718 and 2219 Aluminum. Boeing Co. Report D2-11417, 1969.

60. Speidel, M. O.: Current Understanding of Stress Corrosion Crack Growth in Aluminum Alloys. The Theory of Stress Corrosion Cracking in Alloys, J. C. Scully, ed., NATO Scientific Affairs Division, Brussels, 1971, pp. 289-344.

61. Gest, R. J.; and Troiano, A. R.: Hydrogen Embrittlement and Stress Corrosion Cracking in Aluminum Alloys. L'Hydrogène dans les Métaux, vol. 2, Éditions Science et Industrie, Paris, 1972, pp. 427-432.

62. Gest, R. J.; and Troiano, A. R.: Stress Corrosion and Hydrogen Embrittlement in an Aluminum Alloy. Corrosion, vol. 30, no. 8, Aug. 1974, pp. 274-279.

63. Speidel, Markus O.: Hydrogen Embrittlement of Aluminum Alloys?. Hydrogen in Metals, I. M. Bernstein and Anthony W. Thompson, eds., ASM, 1974, pp. 249-276.

64. Albrecht, J.; McTiernan, B. J.; Bernstein, I. M.; and Thompson, A. W.: Hydrogen Embrittlement in a High-Strength Aluminum Alloy. Scripta Met., vol. 11, no. 10, Oct. 1977, pp. 893-895.

65. Taheri, M.; Albrecht, J.; Bernstein, I. M.; and Thompson, A. W.: Strain Rate Effects on Hydrogen Embrittlement of 7075 Aluminum. Scripta Met., vol. 13, Sept. 1979, pp. 871-875.

66. Albrecht, J.; Thompson, A. W.; and Bernstein, I. M.: The Role of Microstructure in Hydrogen-Assisted Fracture of 7075 Aluminum. Met. Trans. A, vol. 10A, Nov. 1979, pp. 1759-1766.

67. Jacko, R. J.; and Duquette, D. J.: The Role of Hydrogen on Environmental Fatigue of High Strength Aluminum Alloys. ONR Report AD-A090184, Sept. 1980.

68. Marcus, H. L.: Gaseous Environmental Effects on Fatigue Crack Growth. Environmental Degradation of Engineering Materials, M. R. Louthan, Jr. and R. P. McNutt, eds., Virginia Tech, 1977, pp. 41-54.

69. Williams, D. P., III; Pao, P. S.; and Wei, R. P.: The Combined Influence of Chemical, Metallurgical and Mechanical Factors on Environment Assisted Cracking. Environment-Sensitive Fracture of Engineering Materials, Z. A. Foroulis, ed., Metallurgical Soc. of AIME, 1979, pp. 3-15.

70. Weir, T. W.; Simmons, G. W.; Hart, R. G.; and Wei, R. P.: A Model for Surface Reaction and Transport Controlled Fatigue Crack Growth. Scripta Met., vol. 14, no. 3, 1980, pp. 357-364.

71. Pao, P. S.; Wei, W.; and Wei, R. P.: Effect of Frequency on Fatigue Crack Growth Response of AISI 4340 Steel in Water Vapor. Environment-Sensitive Fracture of Engineering Materials, Z. A. Foroulis, ed., Metallurgical Soc. of AIME, 1979, pp. 565-580.

72. Newman, J. C., Jr.: Crack-Opening Displacements in Center-Crack, Compact, and Crack-Line Wedge-Loaded Specimens. NASA TN D-8268, 1976.

73. Standard Test Method for Plane-Strain Fracture Toughness of Metallic Materials. ANSI/ASTM E-399-78a, 1980 Annual Book of ASTM Standards, Part 10, pp. 580-601.

TABLE 1.- CHEMICAL COMPOSITION OF 7475 IN WEIGHT PER CENT

Zn		Mg		Cu		Cr		Fe	Si	Mn	Ti	Others		Al
Max.	Min.	Max.	Min.	Max.	Min.	Max.	Min.	Max.	Max.	Max.	Max.	Each	Total	
6.2	5.2	2.6	1.9	1.9	1.2	0.25	0.18	0.12	0.10	0.06	0.06	0.05	0.15	Bal.

TABLE 2.- PROPERTIES OF 25.4 mm THICK 7475-7651 PLATE

Modulus of elasticity, GPa (a)		Ultimate tensile strength, MPa (a)		0.2% offset yield strength, MPa (a)		Elongation, % in 51 mm (a)		Plane strain fracture toughness, $MN/m^{3/2}$ (b)	
Long.	Trans.	Long.	Trans.	Long.	Trans.	Long.	Trans.	LT	TL
71.7	73.1	572	578	525	515	15.2	14.9	49.9	37.4

[a]Average of 5 tests

[b]One test, as reported by manufacturer

TABLE 3.- EMPIRICAL CONSTANTS FOR FATIGUE CRACK GROWTH RATE CORRELATIONS USING PARIS' CRACK GROWTH LAW, EQUATION (3)

Specimen Orientation	Environment	Water vapor pressure, Pa	Frequency, Hz	C	n
TL	vacuum	- - -	1	9.36×10^{-12}	3.76
LT	↓	- - -	1	2.45×10^{-11}	3.36
TL	↓	- - -	10	1.30×10^{-11}	3.62
LT	↓	- - -	10	2.38×10^{-11}	3.31
↓	lab air	- - -	1	1.02×10^{-10}	3.30
↓	lab air	- - -	10	3.49×10^{-10}	2.67
↓	H_2O vapor/N_2	94	1	1.01×10^{-10}	3.08
↓	↓	150	10	1.83×10^{-10}	2.89
↓	↓	380	1	2.78×10^{-10}	2.77
↓	↓	550	10	2.15×10^{-10}	2.86
↓	↓	1030	1	1.39×10^{-10}	2.99
↓	↓	1020	10	1.24×10^{-10}	3.10
↓	↓	2610	1	9.64×10^{-11}	3.35
↓	↓	2490	10	2.03×10^{-10}	3.00
↓	↓	3150	1	1.27×10^{-10}	3.30
↓	↓	3360	10	2.25×10^{-10}	3.11
↓	↓	3800	1	1.52×10^{-10}	3.30
↓	↓	3600	10	2.50×10^{-10}	3.04

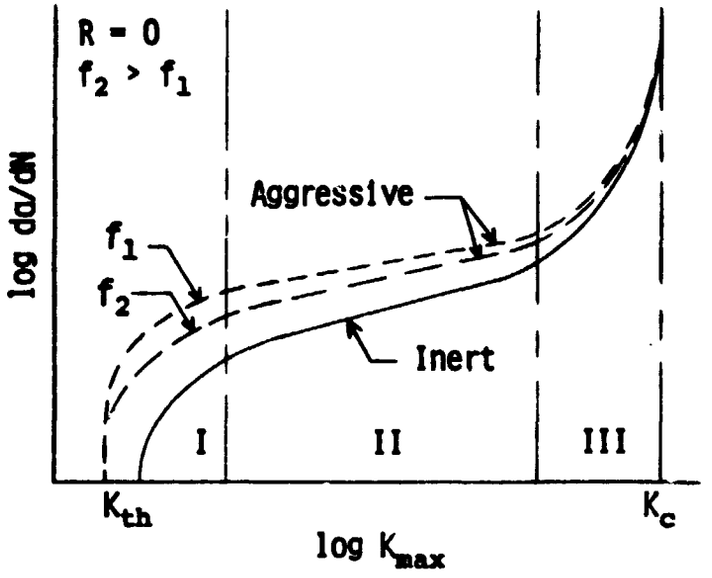

(a) Schematic of corrosion fatigue behavior.

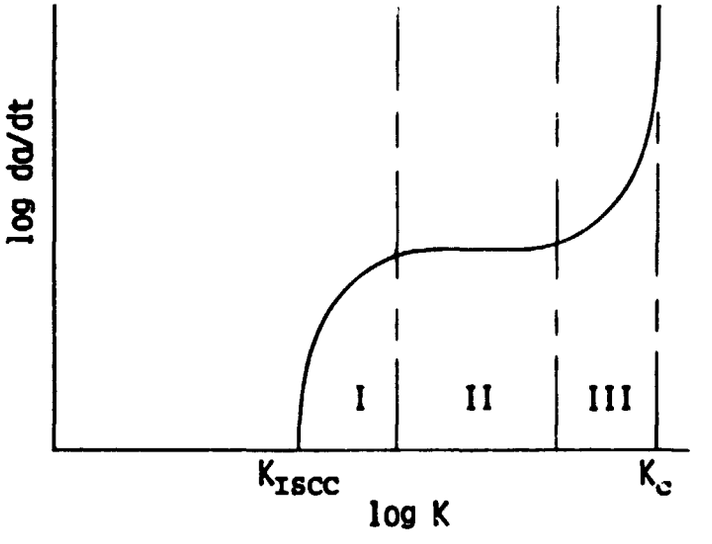

(b) Schematic of stress corrosion cracking behavior.

Figure 1. - Relationship between stress corrosion cracking and corrosion fatigue. (Based on ref. 27.)

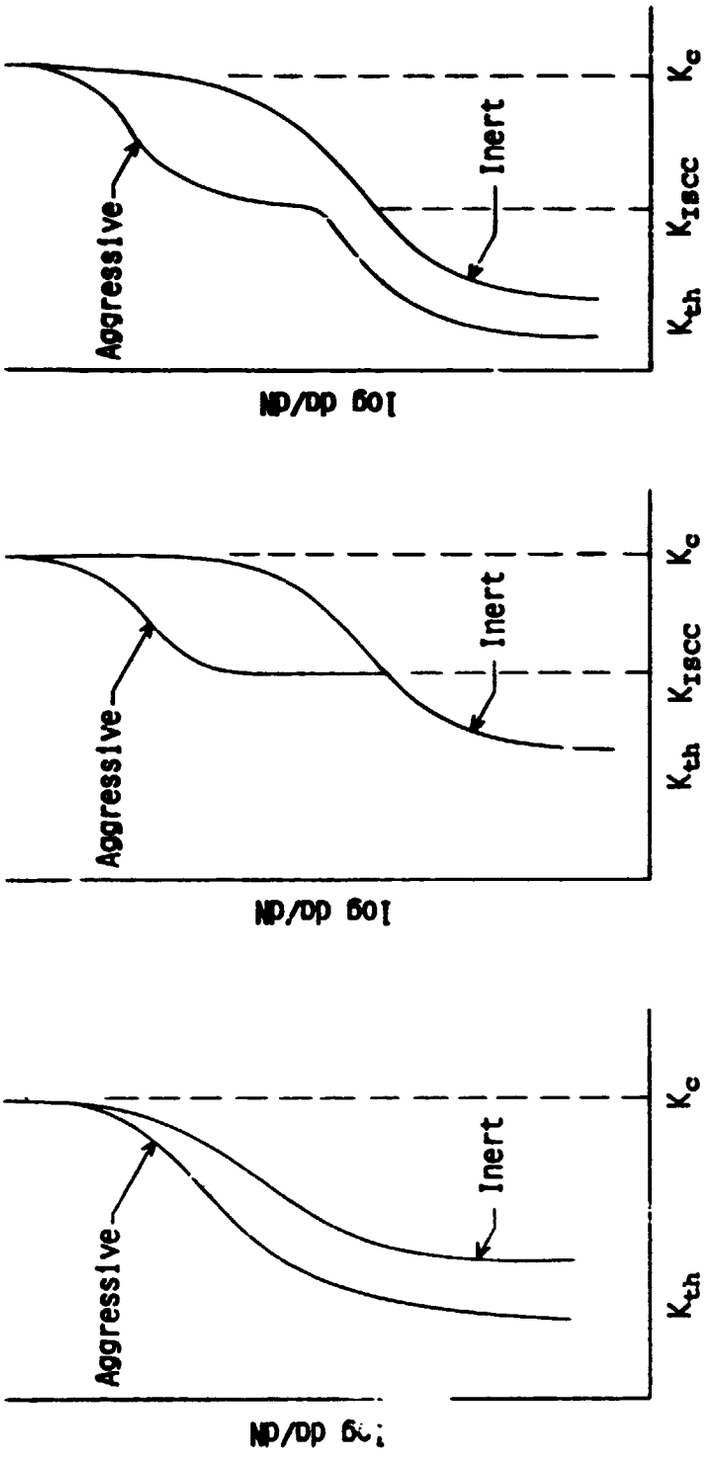

Figure 2. - Types of fatigue crack growth behavior in aggressive environments (ref. 35)

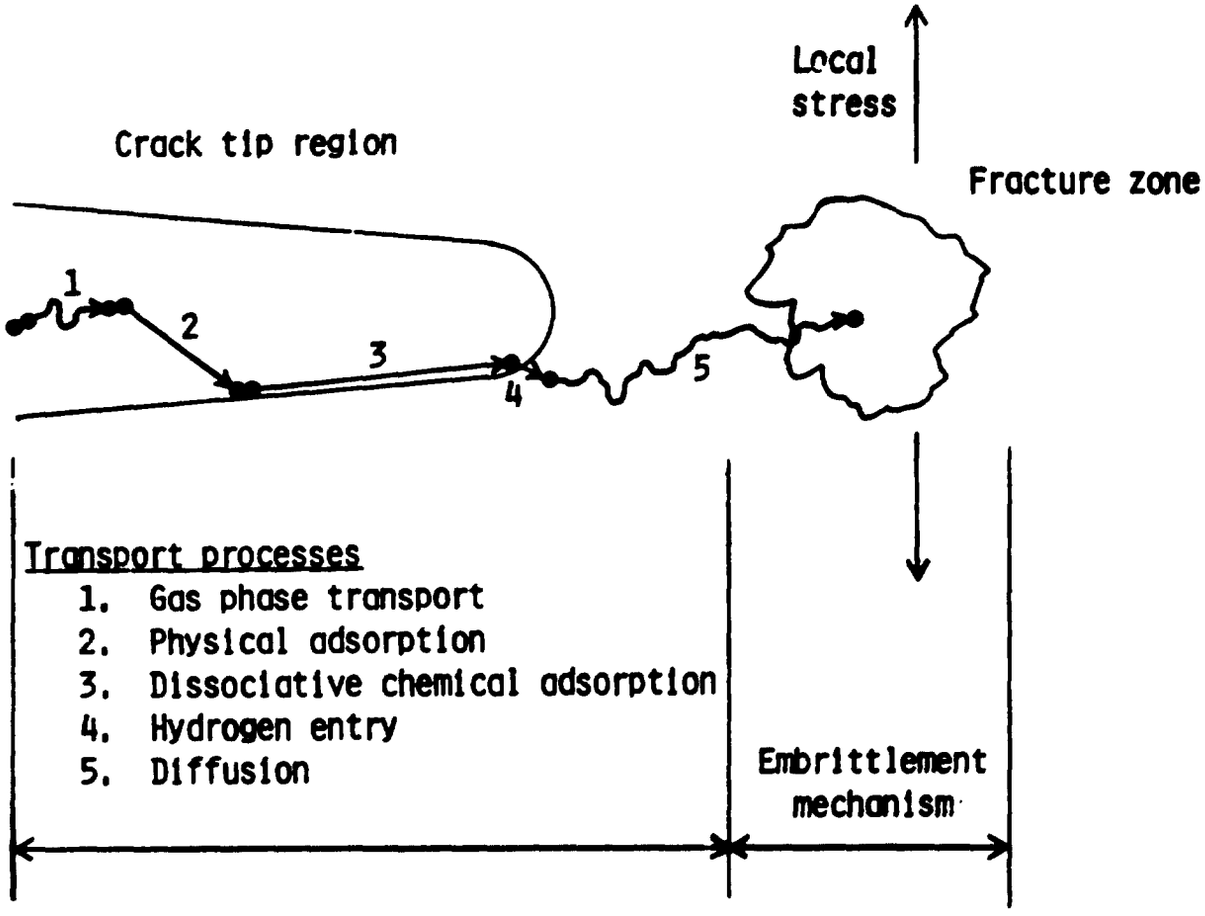

Figure 3. - Schematic of various processes involved in hydrogen embrittlement of aluminum alloys during fatigue in water vapor. (Based on ref. 69.)

(a) Longitudinal section.

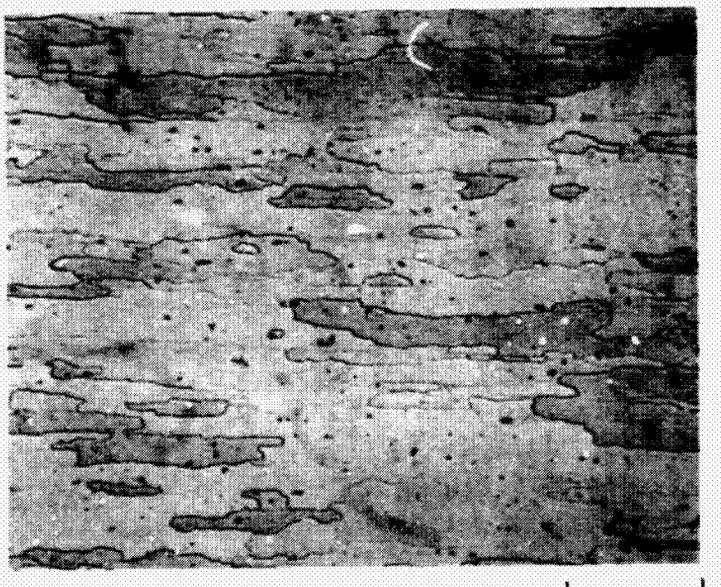

(b) Transverse section.

Figure 4.- Microstructure of 7475-T651 plate.

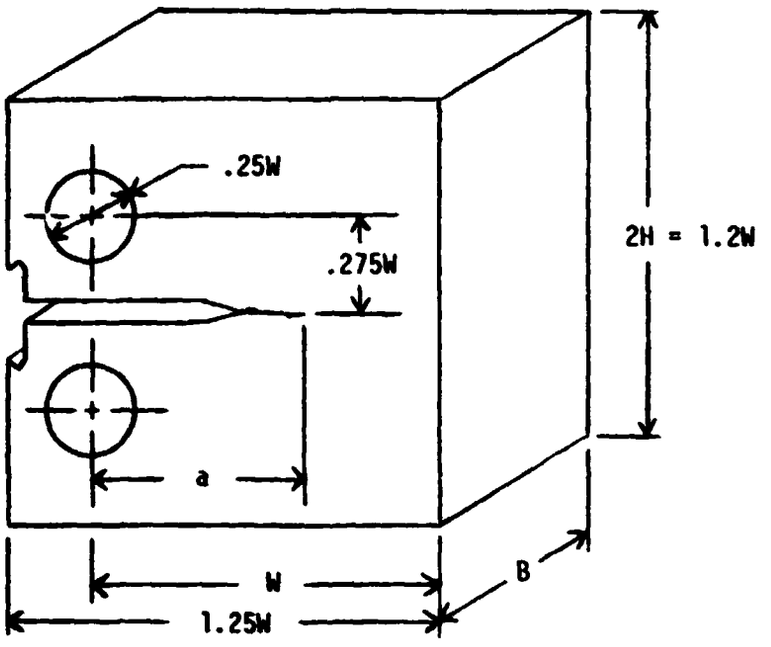

(a) Standard proportions and nomenclature

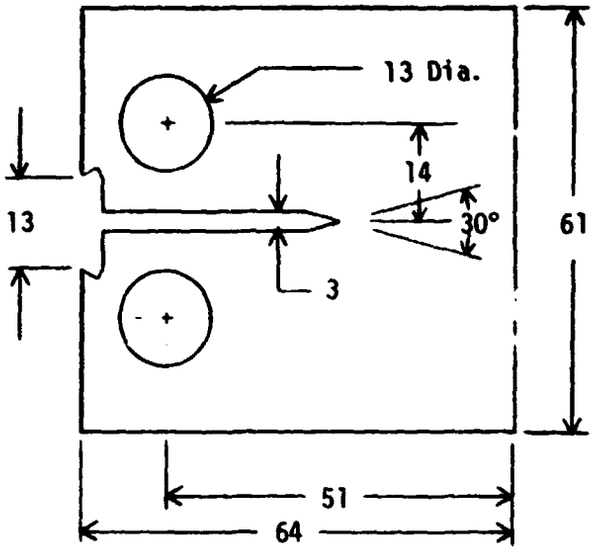

(b) Test specimen (dimensions in mm)
B = 25 mm nominal

Figure 5. - CT specimen configuration.

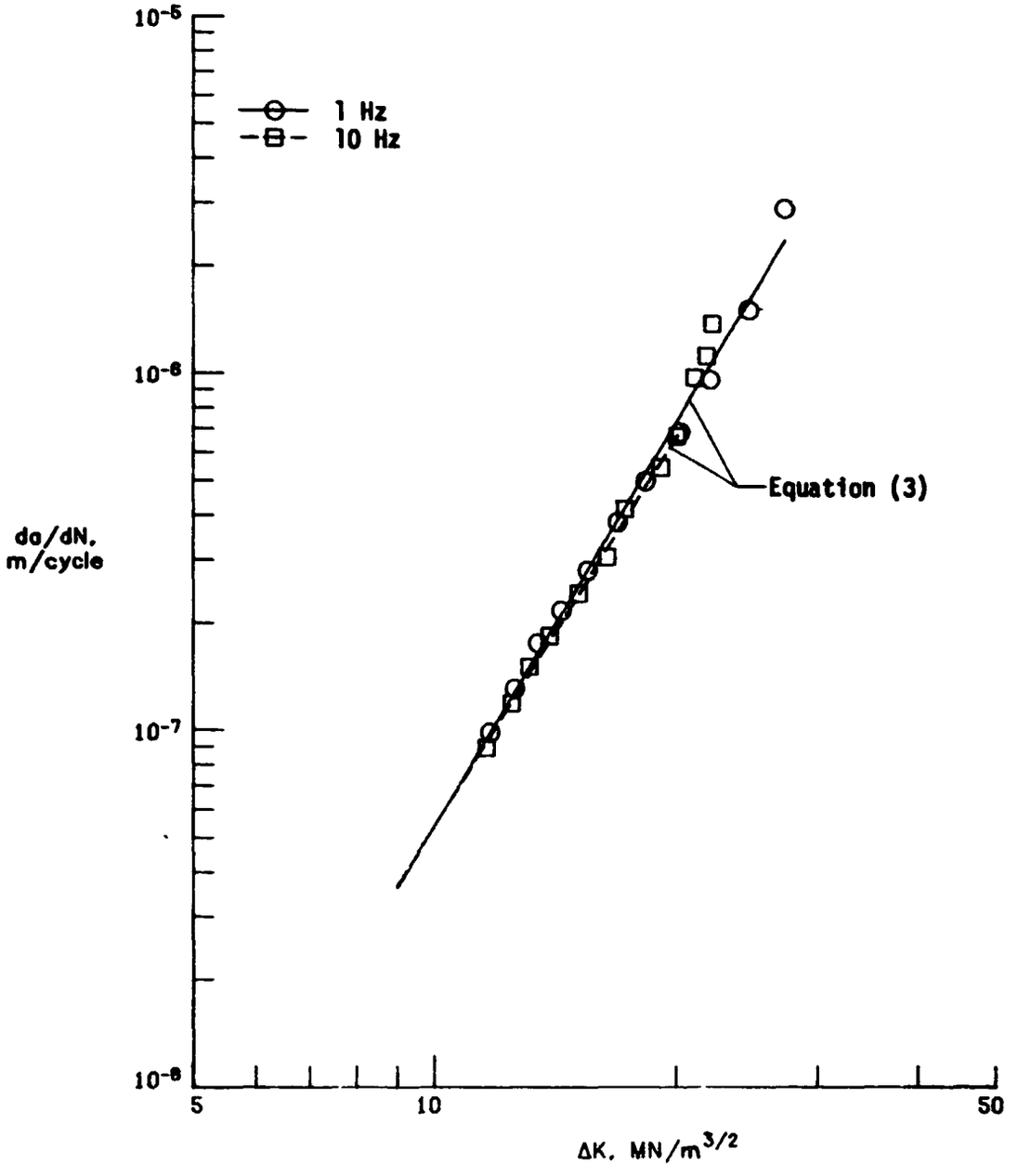

Figure 6. - Fatigue crack growth rates in the TL orientation for 7475-T651 in a vacuum of 130 μPa at frequencies of 1 Hz and 10 Hz. R = 0.2.

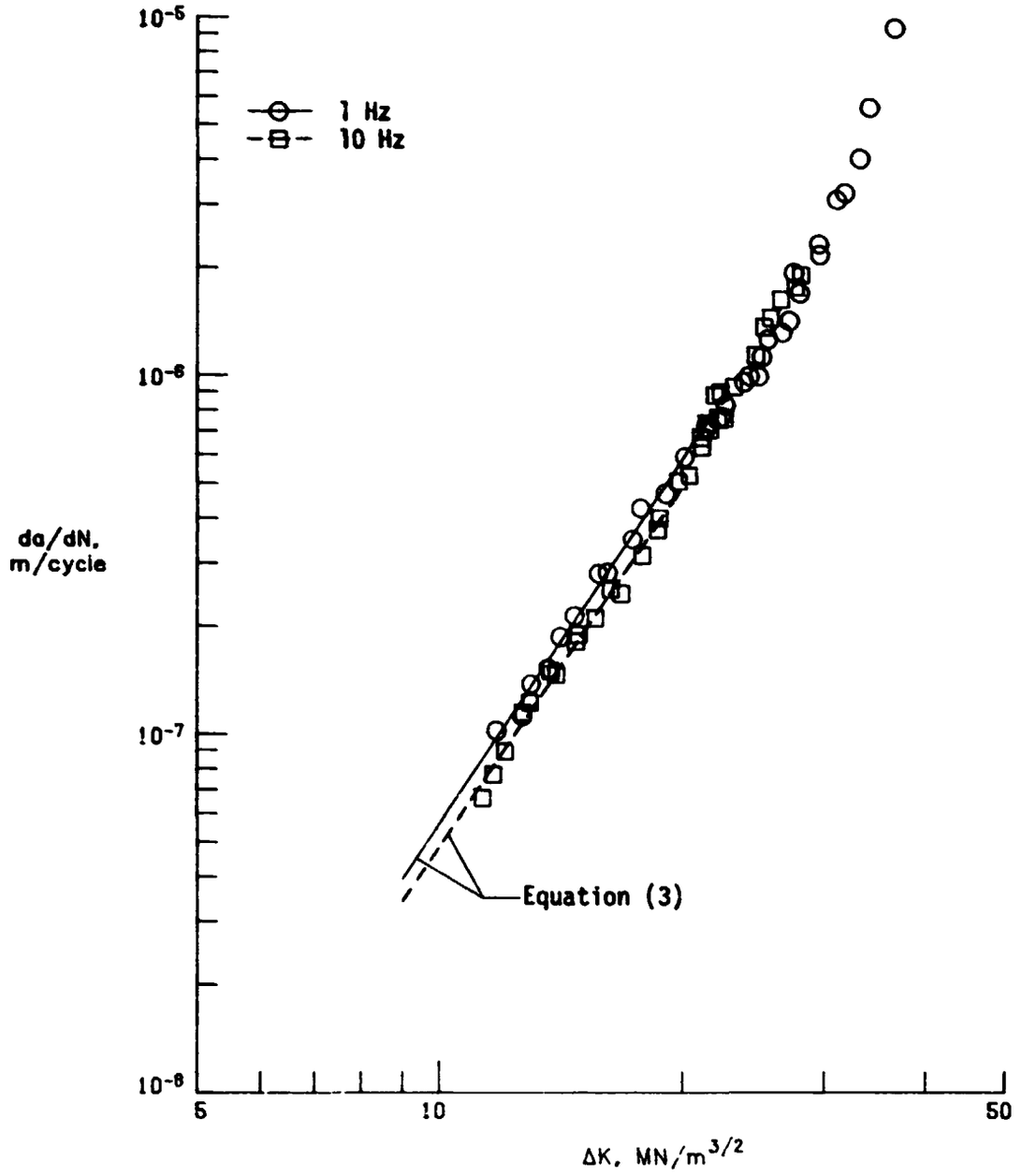

Figure 7. - Fatigue crack growth rates in the LT orientation for 7475-T651 in a vacuum of 130 μPa at frequencies of 1 Hz and 10 Hz. R = 0.2.

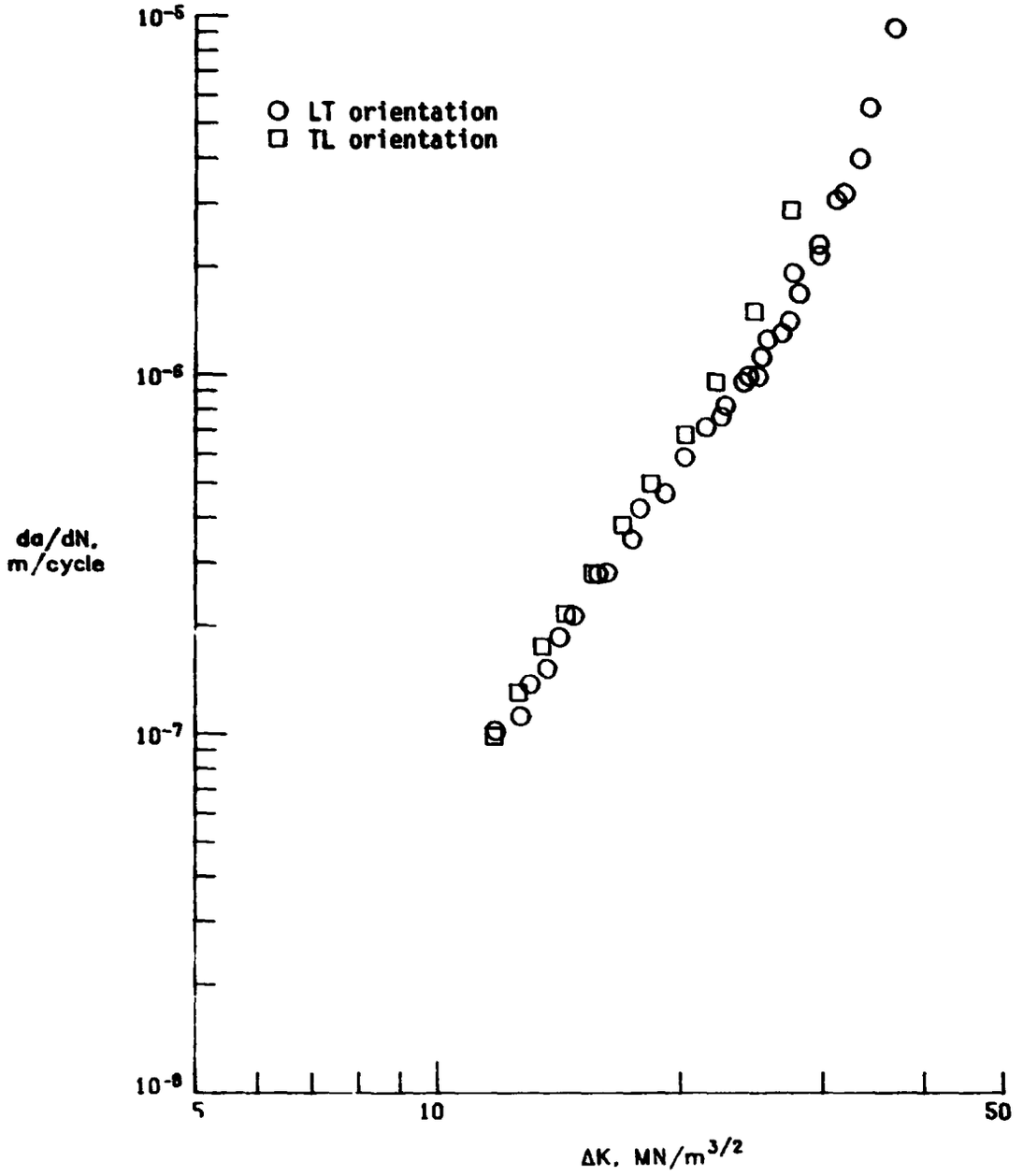

Figure 8. - Comparison of fatigue crack growth rates in the TL and LT orientations for 7475-T651 in a vacuum of 130 μPa at a frequency of 1 Hz. R = 0.2.

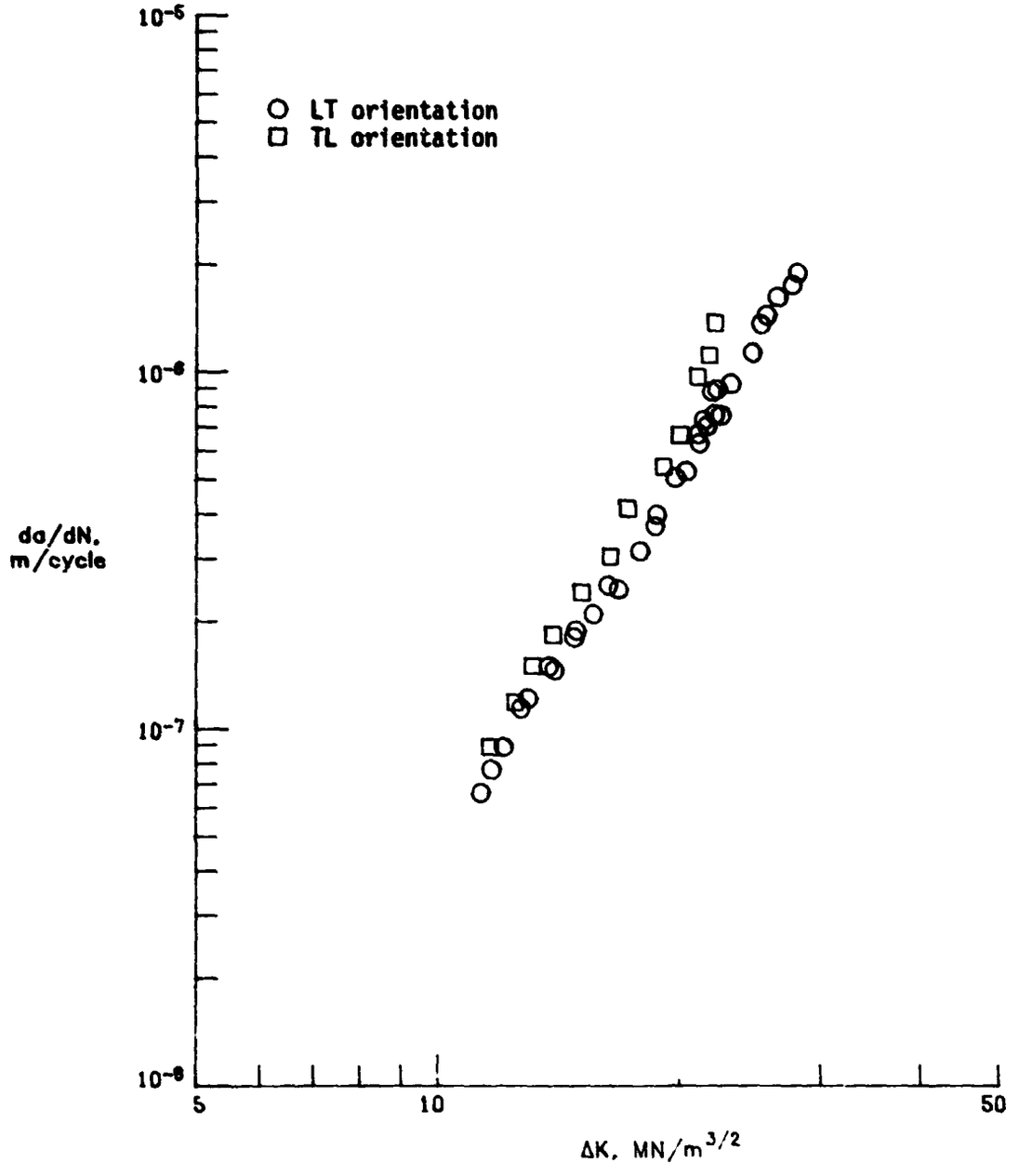

Figure 9. - Comparison of fatigue crack growth rates in the TL and LT orientations for 7475-T651 in a vacuum of 130 μPa at a frequency of 10 Hz. R = 0.2.

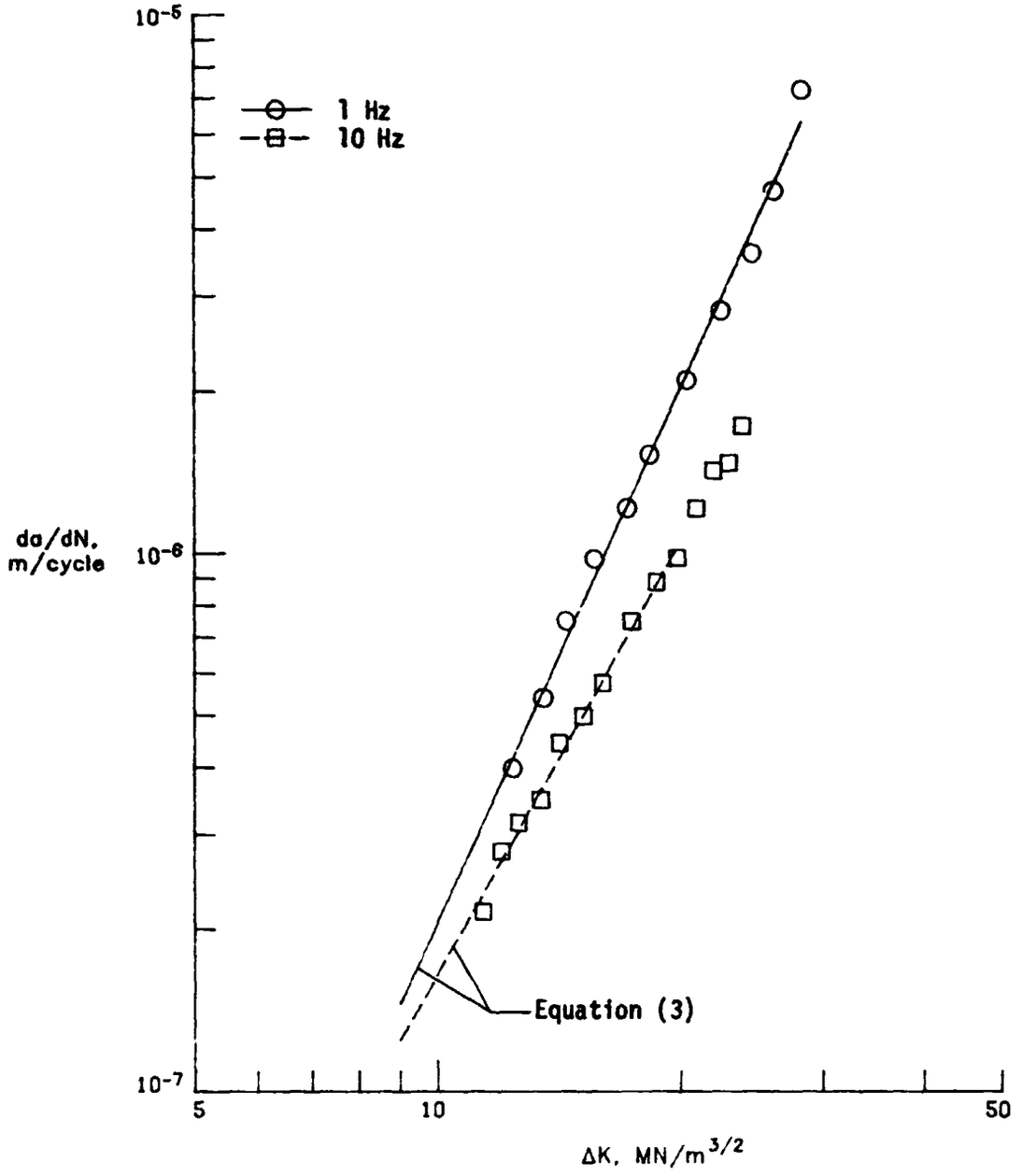

Figure 10. - Fatigue crack growth rates for 7475-T651 in laboratory air at frequencies of 1 Hz and 10 Hz. LT orientation; R = 0.2.

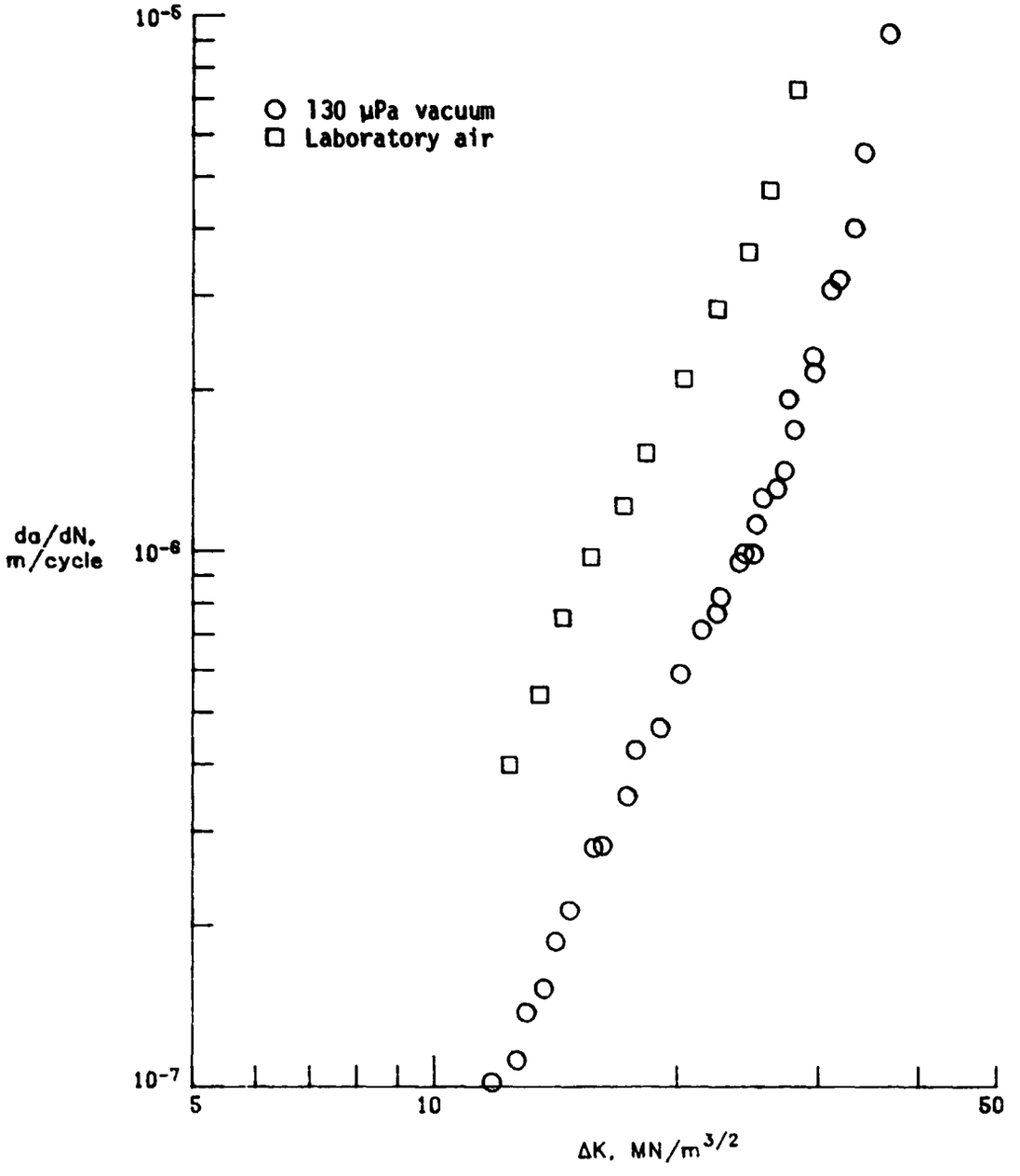

Figure 11. - Comparison of fatigue crack growth rates for 7475-T651 in laboratory air and in a vacuum of 130 μPa at a frequency of 1 Hz. L-T orientation; R = 0.2.

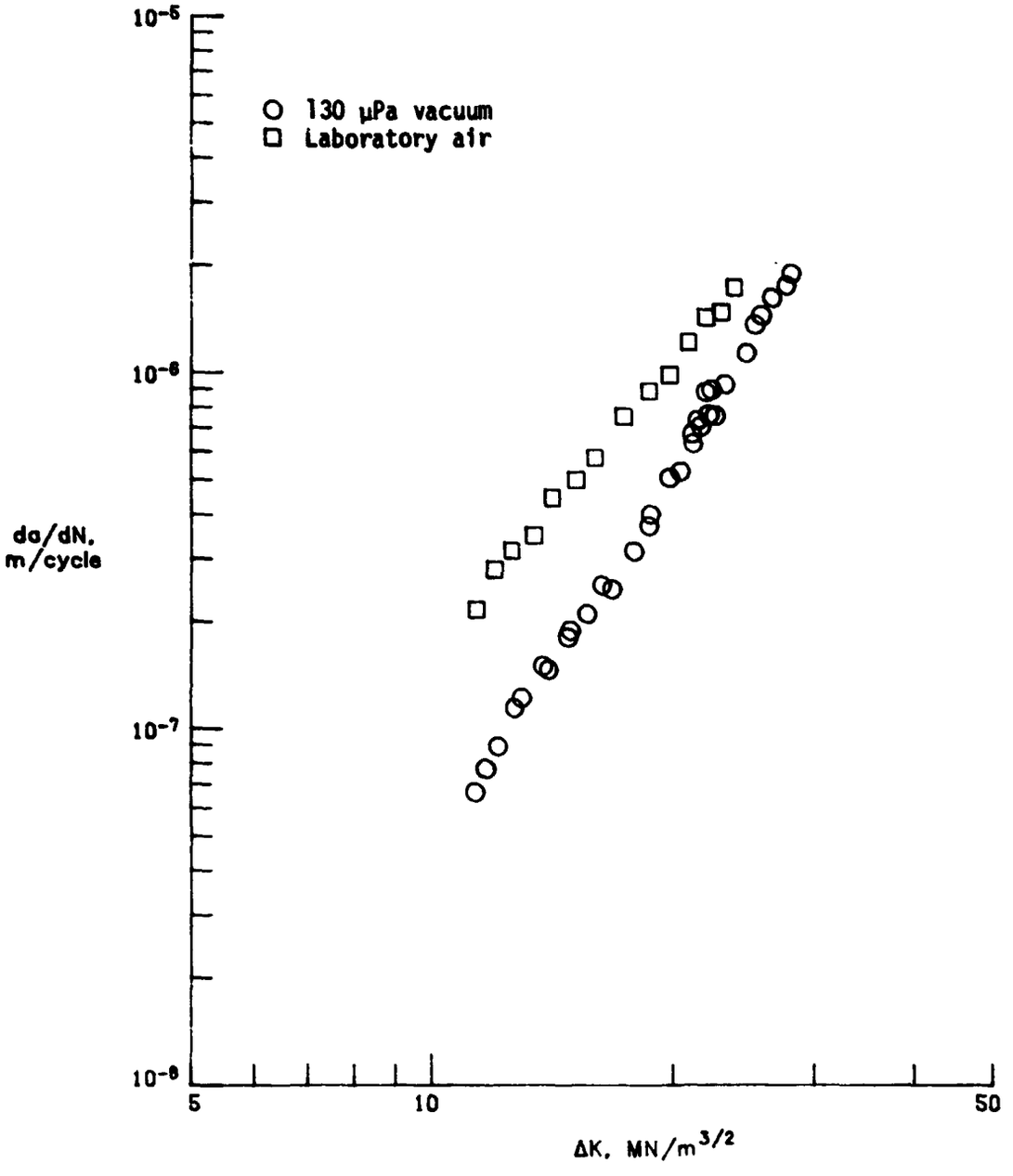

Figure 12. - Comparison of fatigue crack growth rates for 7475-T651 in laboratory air and in a vacuum of 130 μPa at a frequency of 10 Hz. LT orientation; R = 0.2.

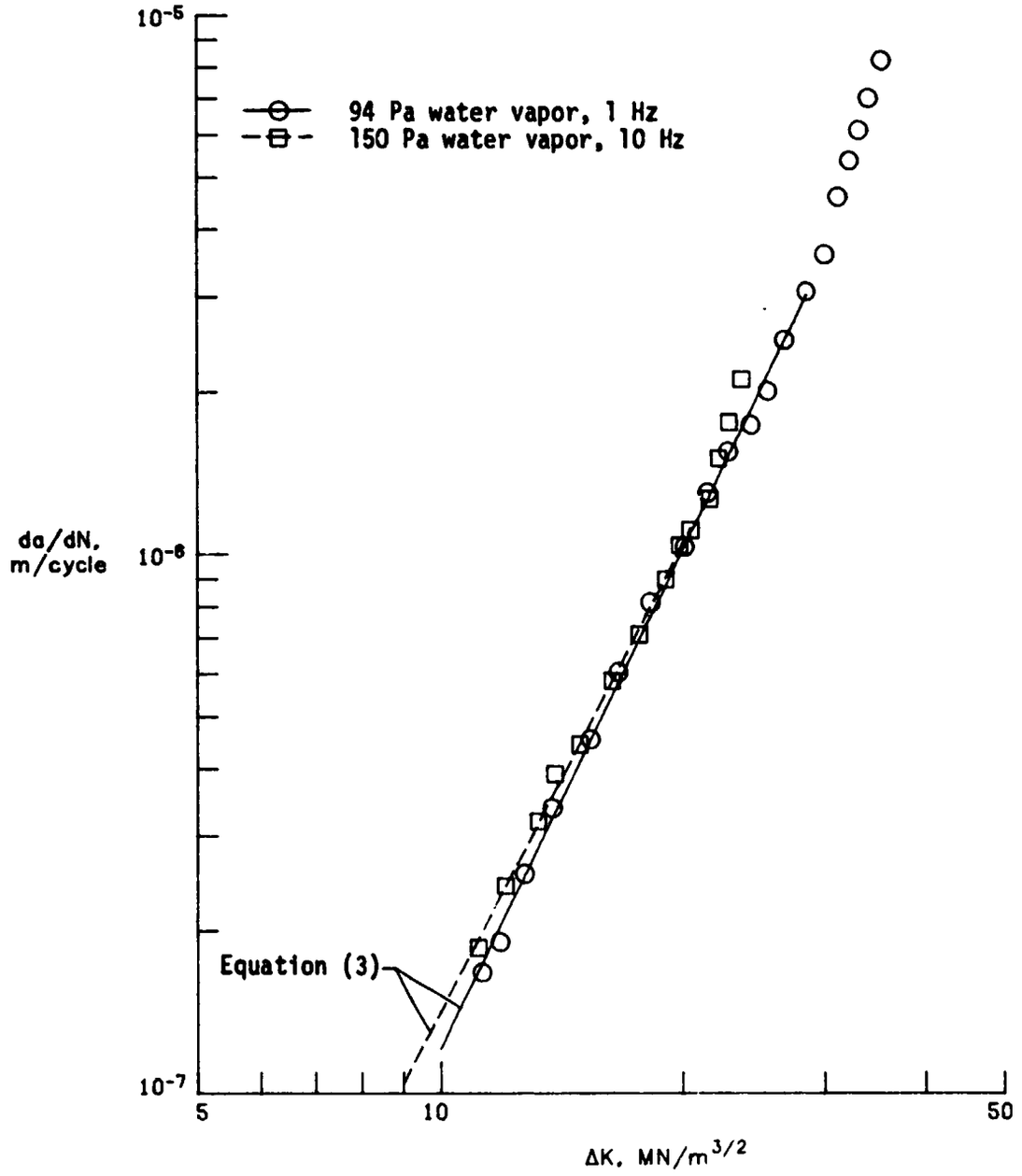

Figure 13. - Fatigue crack growth rates for 7475-T651 at water vapor pressures of 94-150 Pa at frequencies of 1 Hz and 10 Hz. LT orientation; R = 0.2.

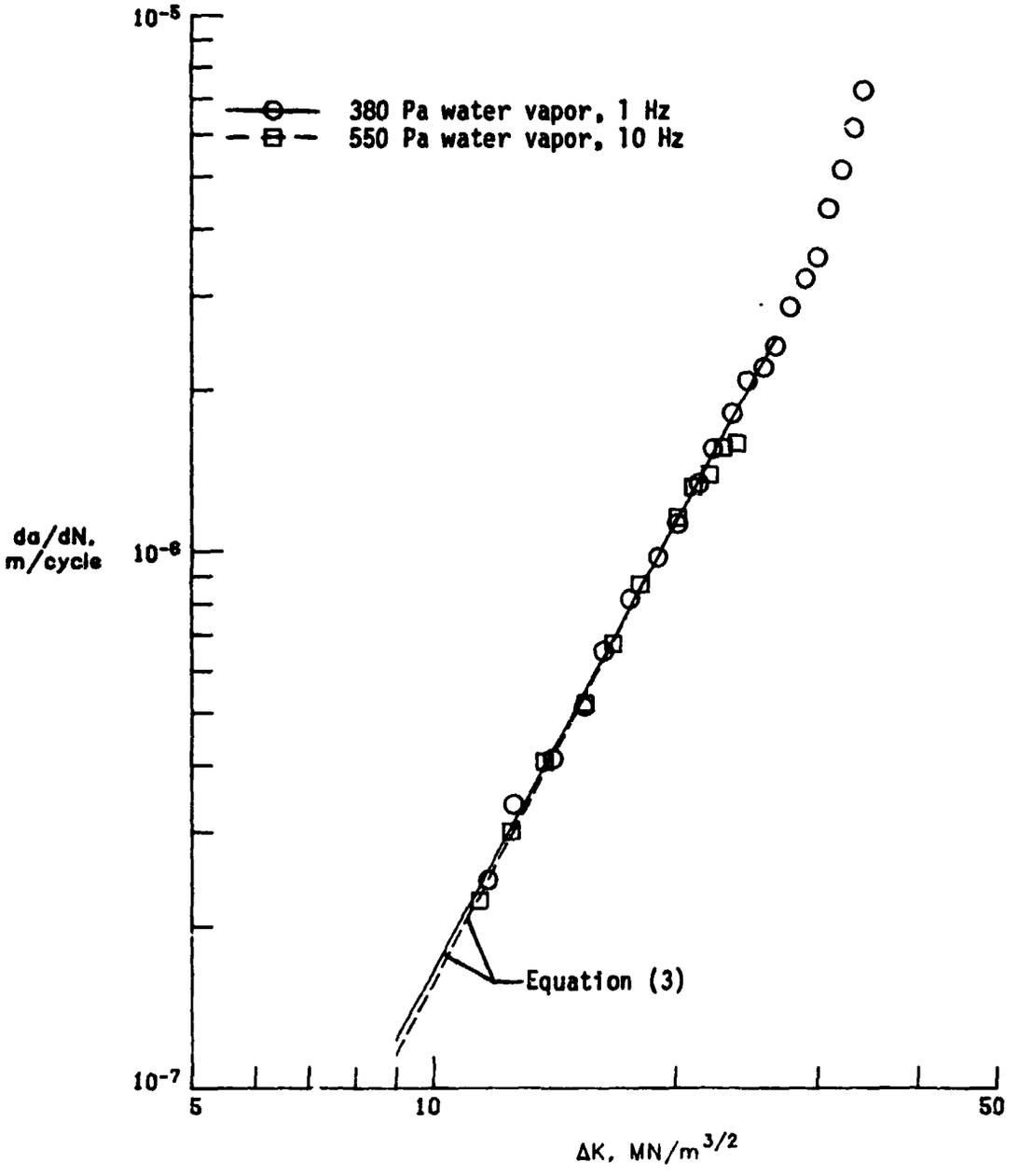

Figure 14. - Fatigue crack growth rates for 7475-T651 at water vapor pressures of 380-550 Pa at frequencies of 1 Hz and 10 Hz. LT orientation; R = 0.2.

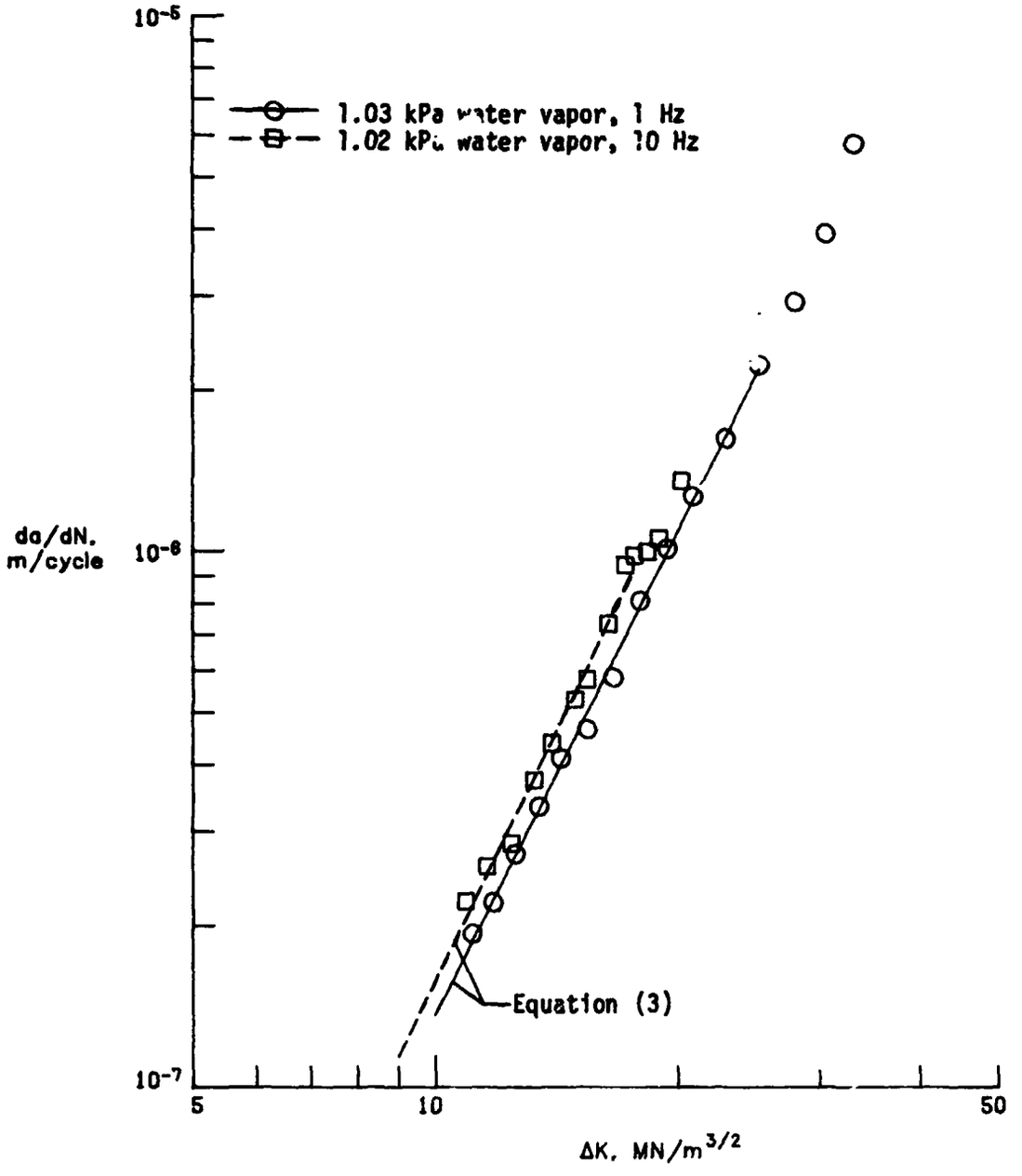

Figure 15. - Fatigue crack growth rates for 7475-T651 at water vapor pressures of 1.02-1.03 kPa at frequencies of 1 Hz and 10 Hz. LT orientation; R = 0.2.

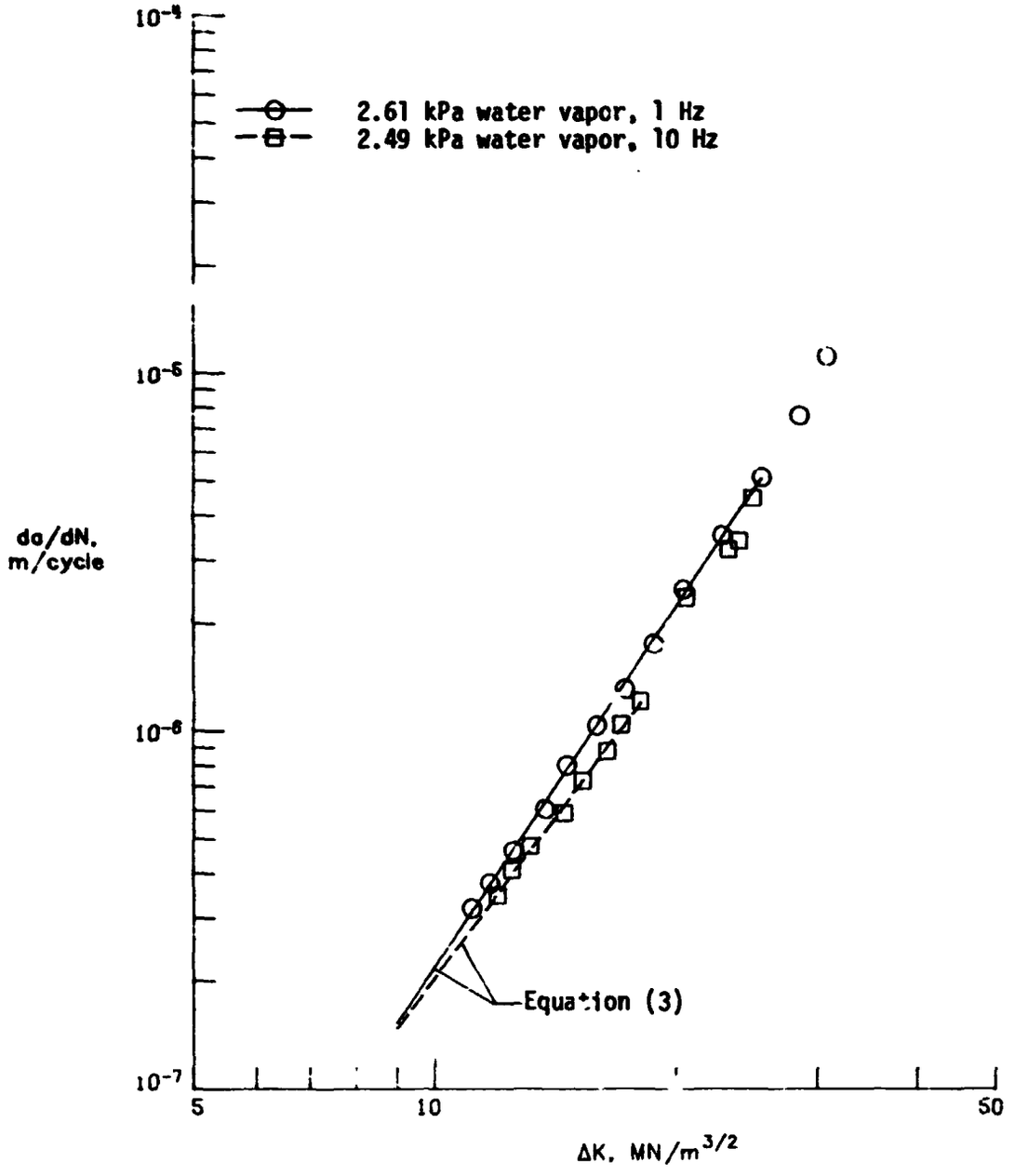

Figure 16. - Fatigue crack growth rates for 7475-T651 at water vapor pressures of 2.49-2.61 kPa at frequencies of 1 Hz and 10 Hz. LT orientation; R = 0.2.

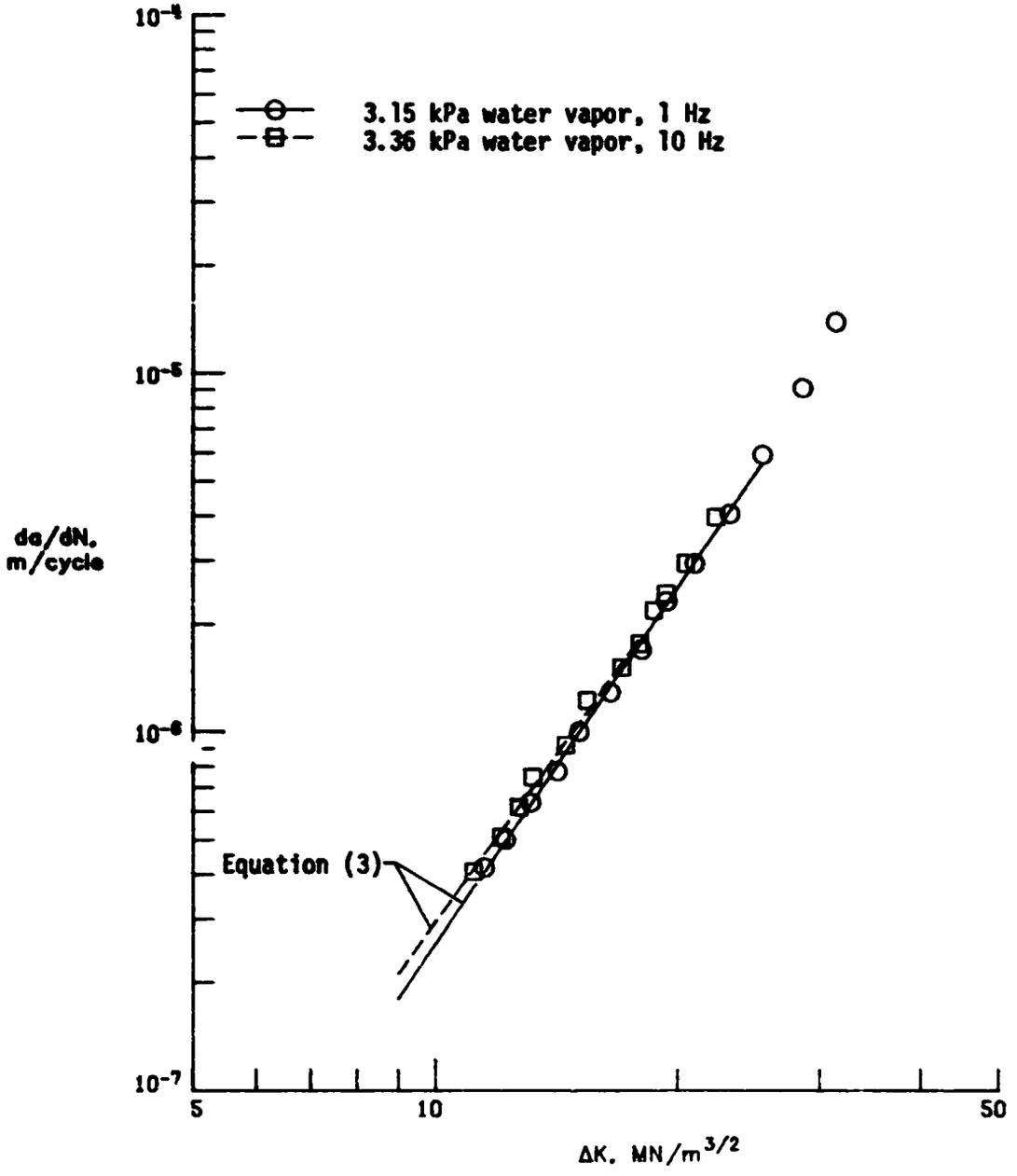

Figure 17. - Fatigue crack growth rates for 7475-T651 at water vapor pressures of 3.15-3.36 kPa at frequencies of 1 Hz and 10 Hz. LT orientation; R = 0.2.

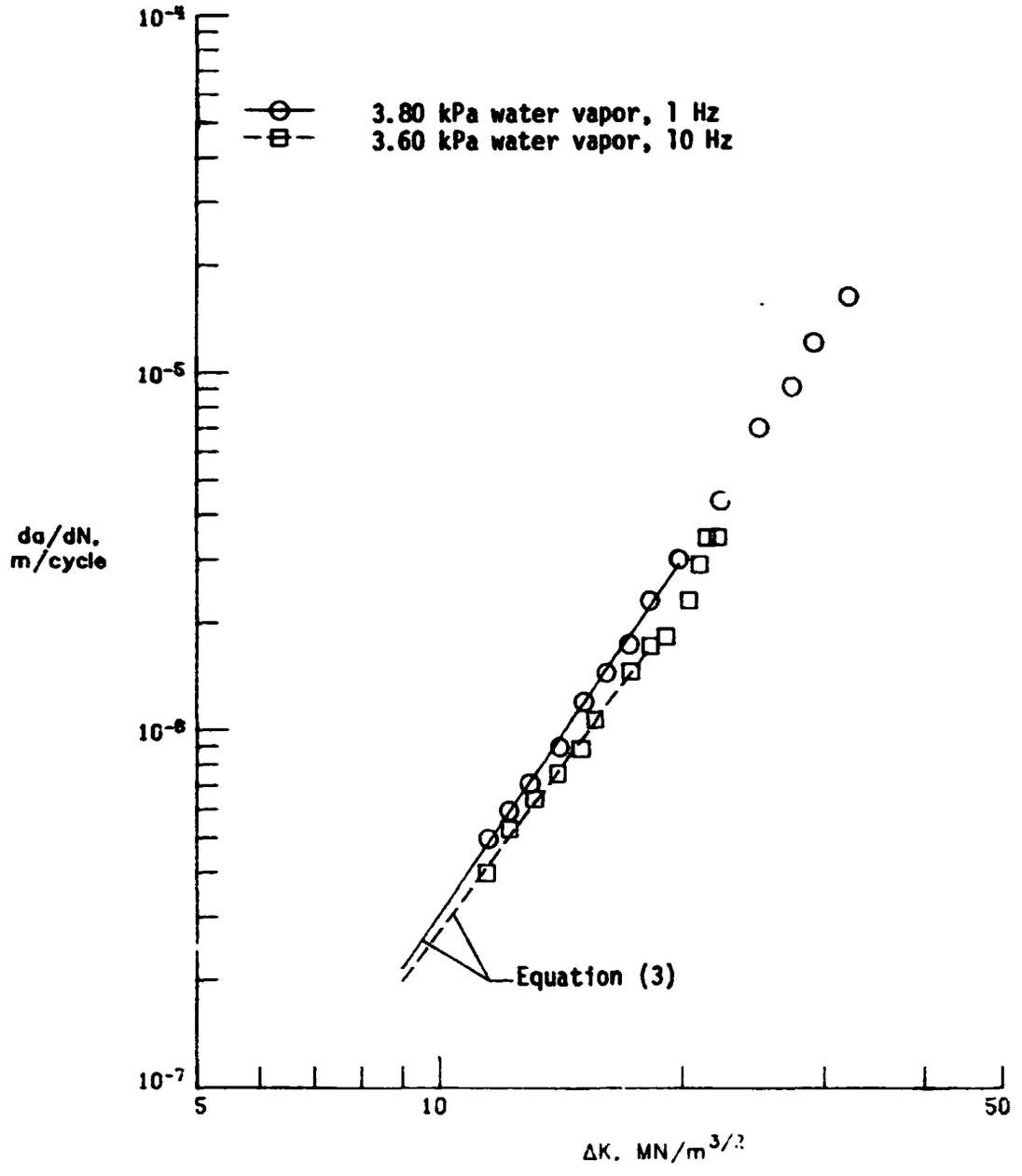

Figure 18. - Fatigue crack growth rates for 7475-T651 at water vapor pressures of 3.60-3.80 kPa at frequencies of 1 Hz and 10 Hz. LT orientation; R = 0.2.

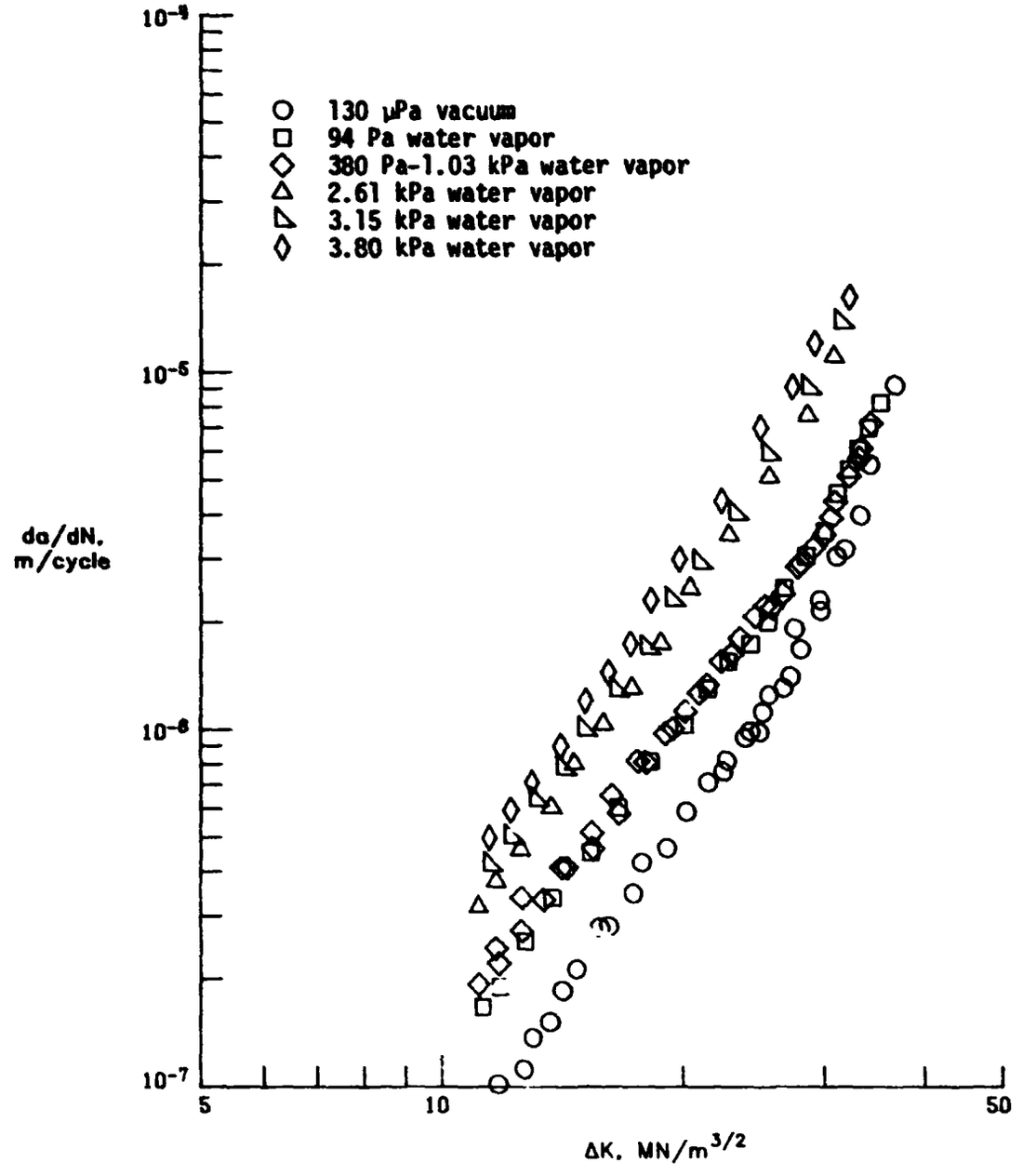

Figure 19. - Comparison of fatigue crack growth rates for 7475-T651 at various water vapor pressures and in a vacuum of 130 μPa at a frequency of 1 Hz. LT orientation; R = 0.2.

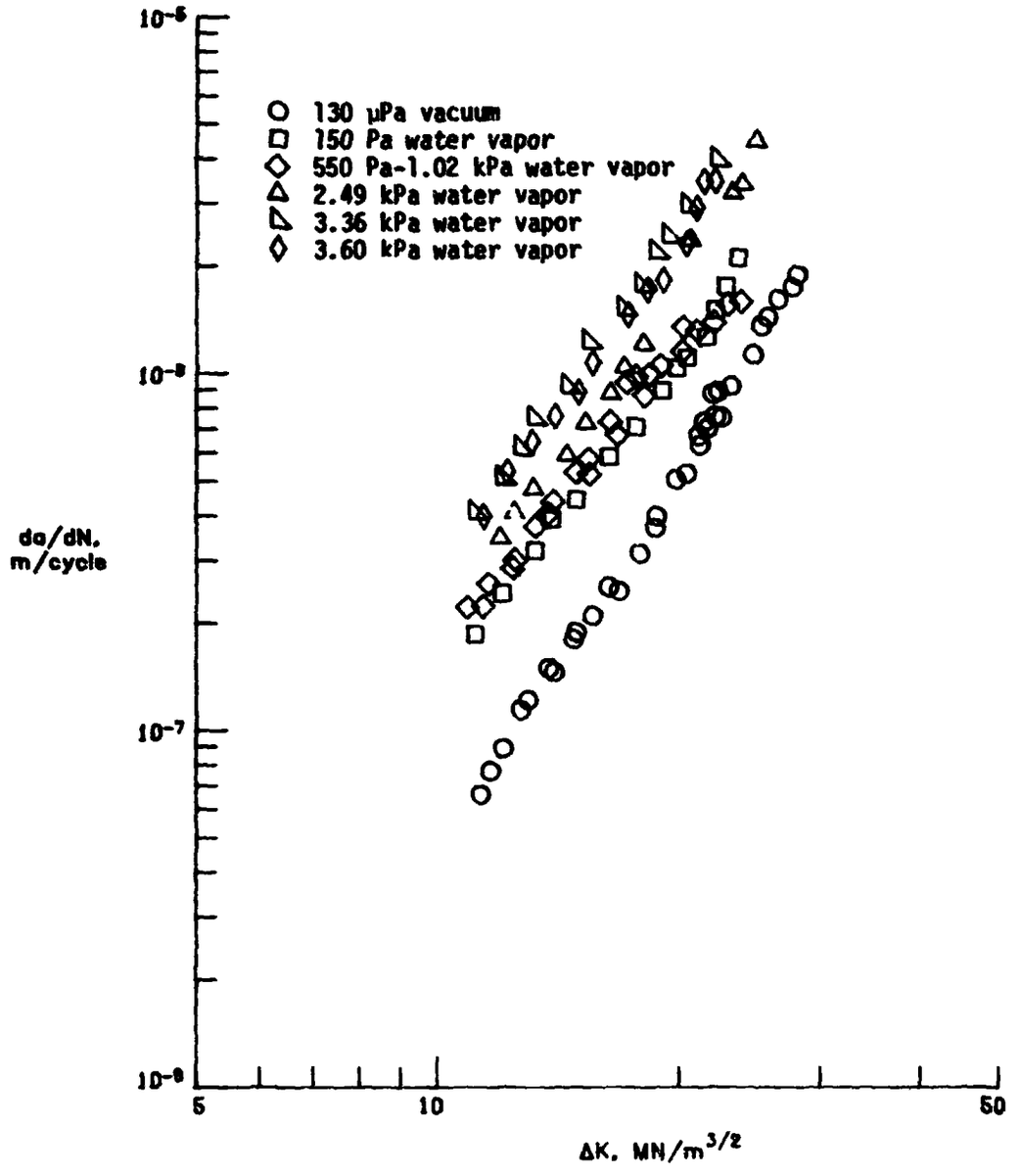

Figure 20. - Comparison of fatigue crack growth rates for 7475-T651 at various water vapor pressures and in a vacuum of 130 μPa at a frequency of 10 Hz. LT orientation; R = 0.2.

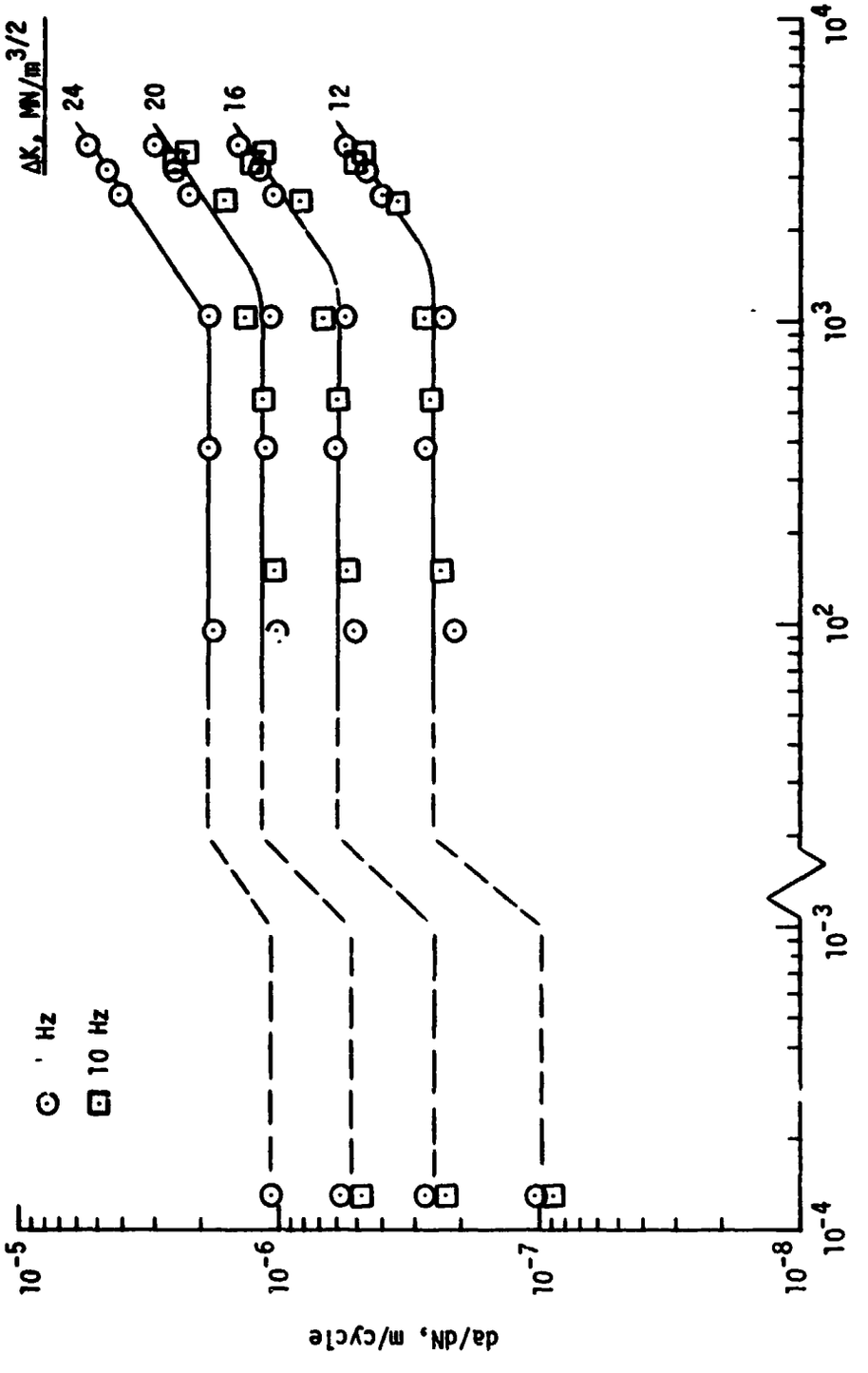

Figure 21. - Variation of da/dN with water vapor pressure for 7475-T651 at constant ΔK values. LT orientation; R = 0.2.

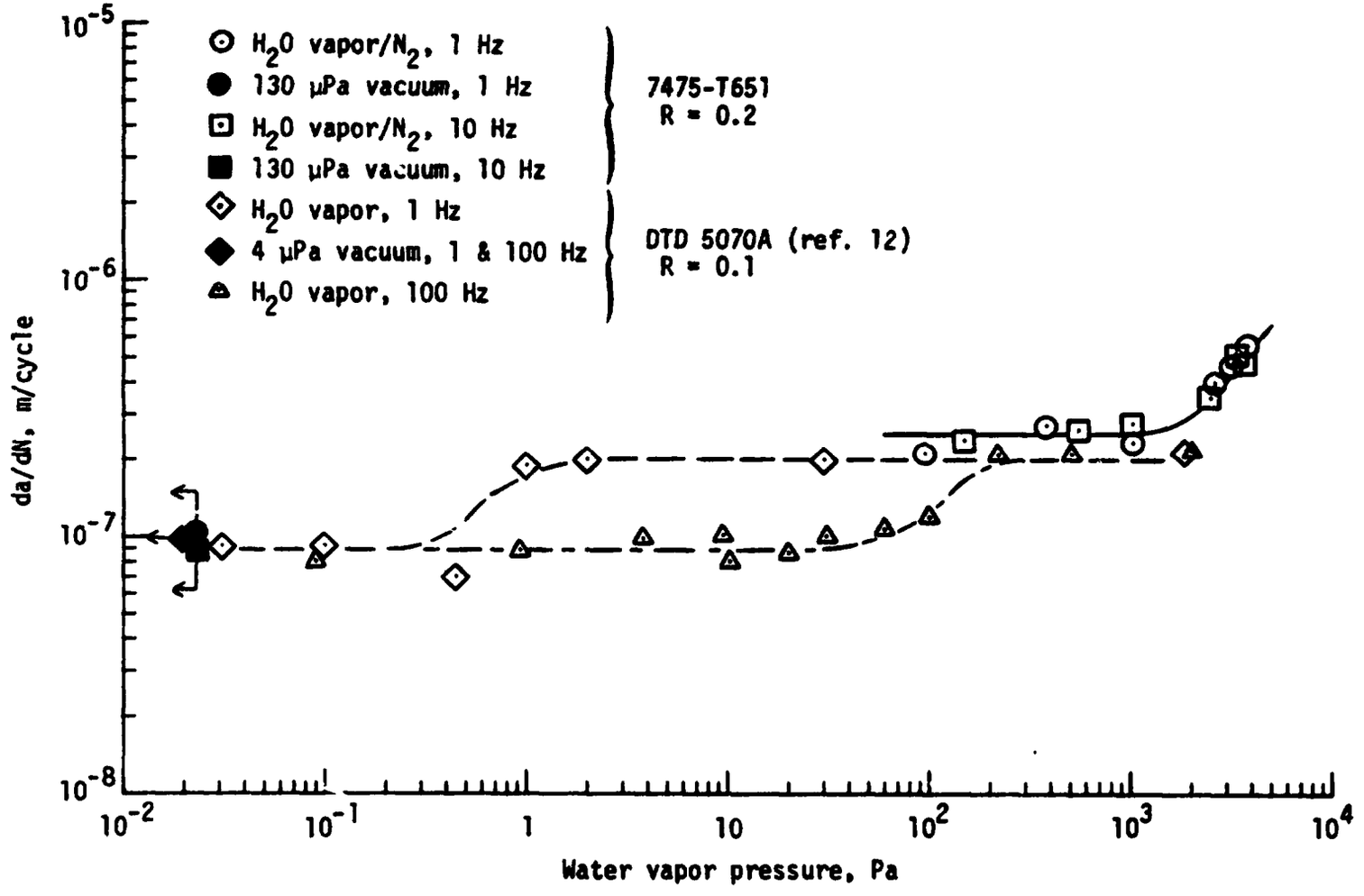

Figure 22. - Comparison of the variation of da/dN with water vapor pressure in 7475-T651 and DTD 5070A at $\Delta K = 12$ MN/m$^{3/2}$.

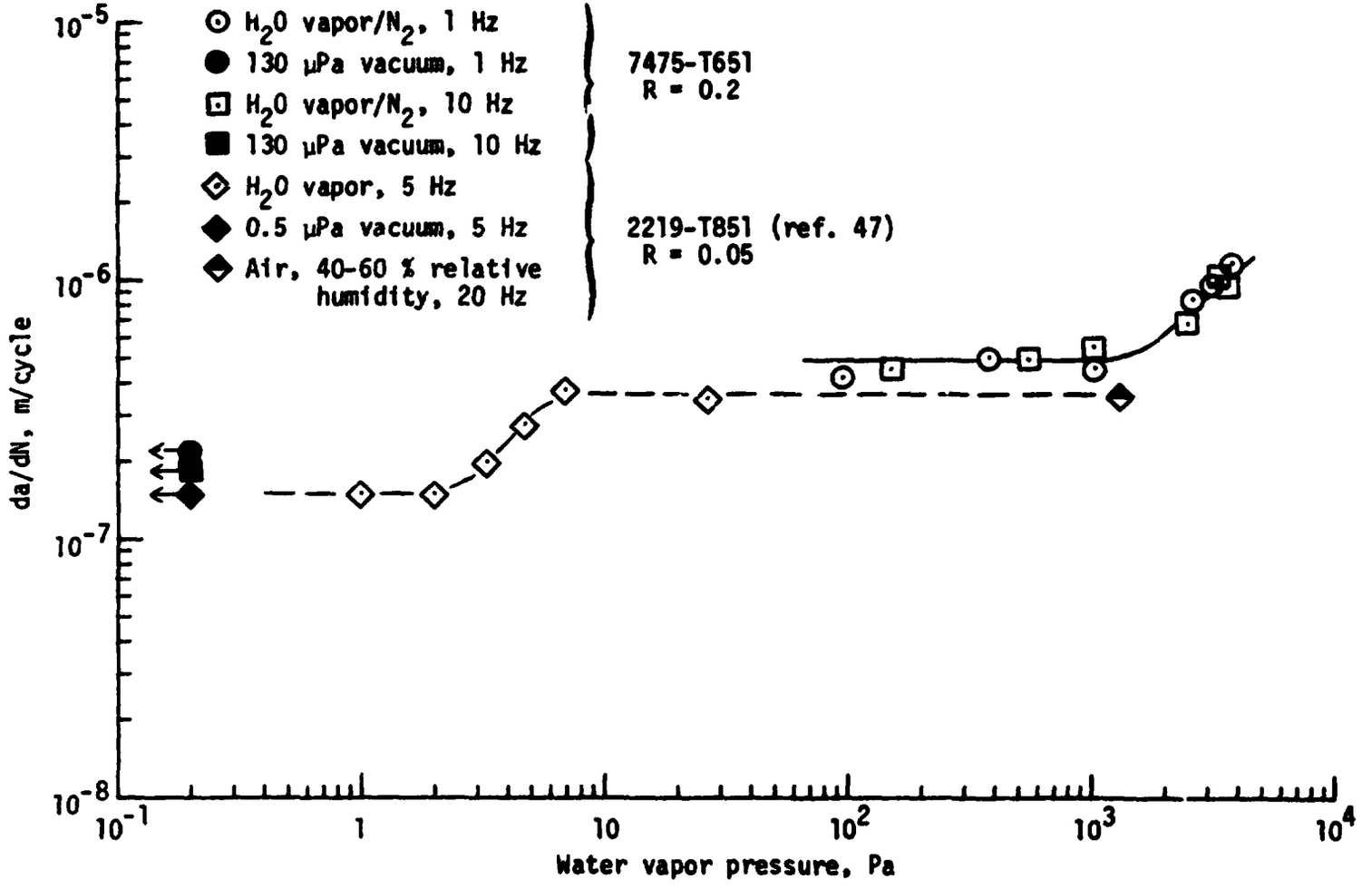

Figure 23. - Comparison of the variation of da/dN with water vapor pressure for 7475-T651 and 2219-T851 at $\Delta K = 15$ MN/m$^{3/2}$.

Figure 24. - Optical macrographs of fracture surfaces of 7475-T651 specimens fatigued in vacuum.

(a) 150 Pa (b) 3.6 kPa

Figure 25. - Optical macrographs of fracture surfaces of 7475-T651 specimens fatigued at low and high water vapor pressure.

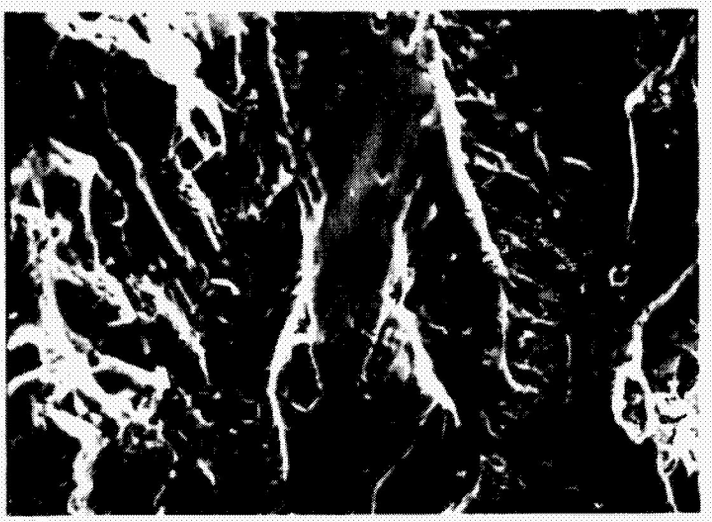

(a) 3.6 kPa H_2O vapor. ΔK = 11 $MN/m^{3/2}$.

(b) Vacuum. ΔK = 13 $MN/m^{3/2}$.

Figure 26. - Scanning electron fractographs of low ΔK regions of 7475-T651 specimens tested in water vapor and vacuum.

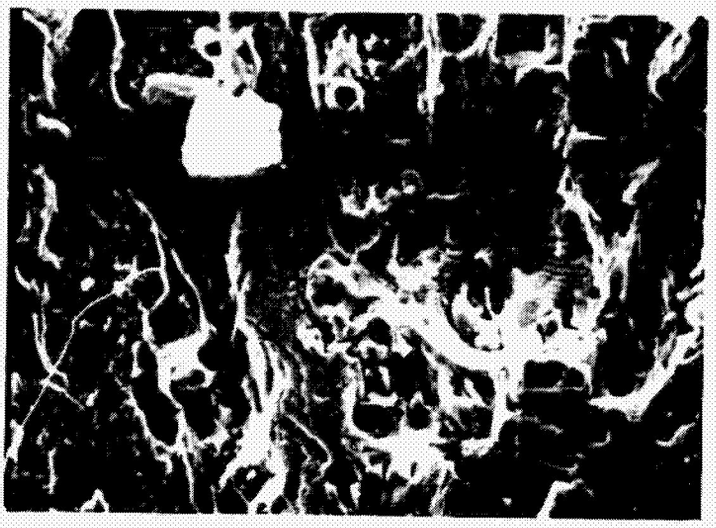

(a) 3.6 kPa H_2O vapor. $\Delta K = 23\ MN/m^{3/2}$.

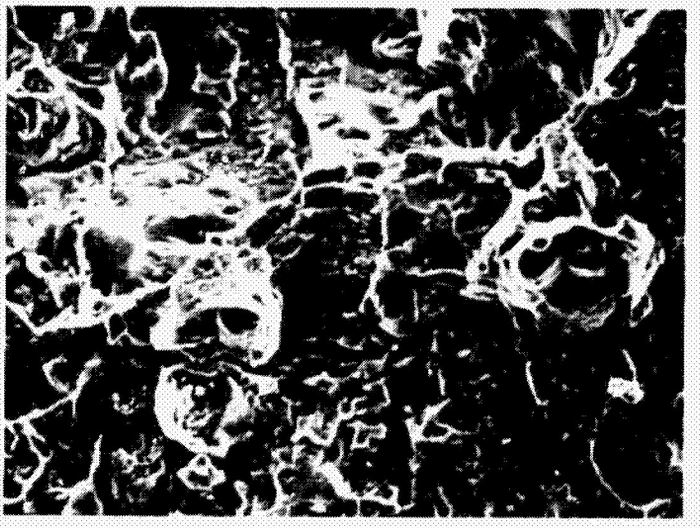

(b) Vacuum. $\Delta K = 22\ MN/m^{3/2}$.

Figure 27. - Scanning electron fractographs of high ΔK regions of 7475-T651 specimens tested in water vapor and vacuum.

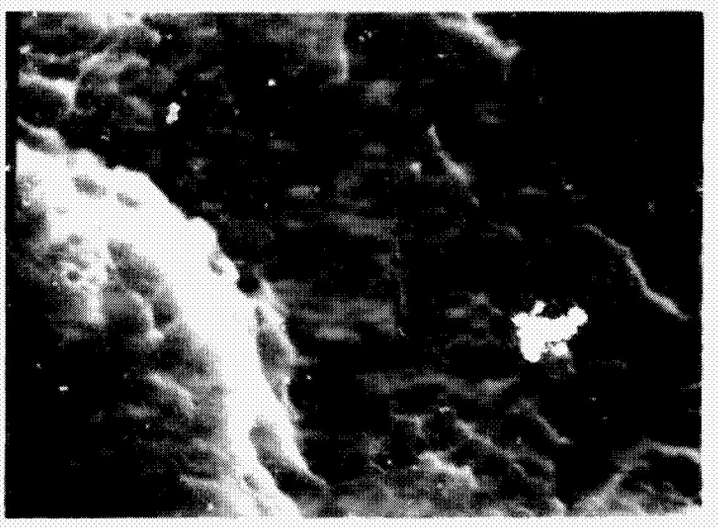

(a) 3.6 kPa H_2O vapor. ΔK = 22 $MN/m^{3/2}$.

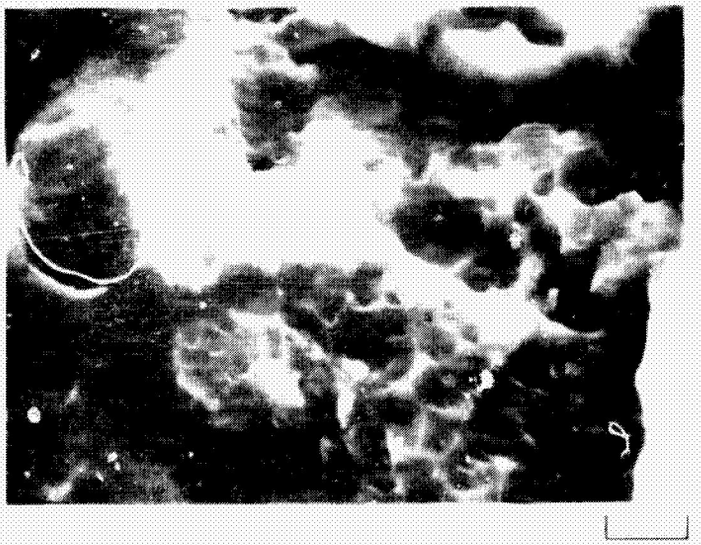

(b) Vacuum. ΔK = 22 $MN/m^{3/2}$.

Figure 28. - High magnification scanning electron fractographs showing small patches of fine dimpled rupture found in high ΔK regions of 7475-T651 tested in water vapor and vacuum.

(a) 94 Pa water vapor. $\Delta K = 14\ MN/m^{3/2}$.

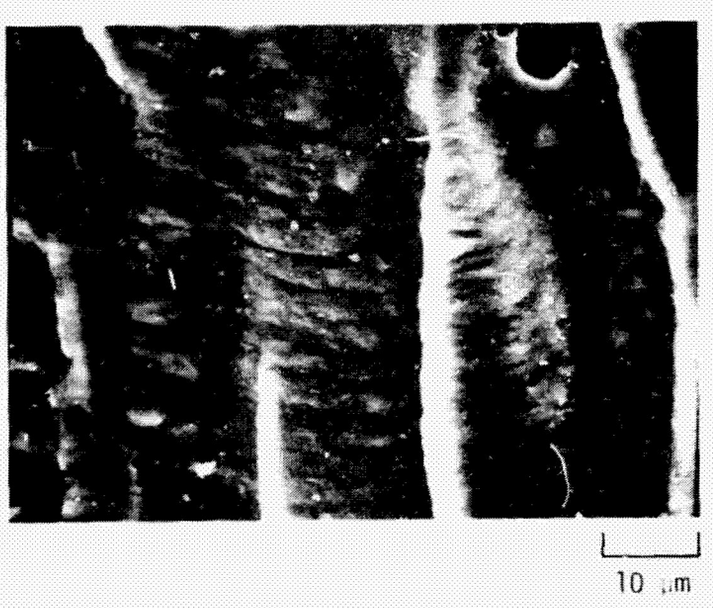

(b) Vacuum. $K = 15\ MN/m^{3/2}$.

Figure 29. - Scanning electron fractographs of fatigue striations formed on 7475-T651 specimens tested in water vapor and vacuum.

(a) ΔK = 15 $MN/m^{3/2}$.

(b) ΔK = 18 $MN/m^{3/2}$.

Figure 30. - Scanning fractographs showing regions of transverse cracking on 7475-T651 specimens tested in vacuum.

C-2